Kinematic history of western Marie Byrd Land, West Antarctica: direct evidence from Cretaceous mafic dykes

CHRISTINE S. SIDDOWAY[1], LOUIS C. SASS III[1] & RICHARD P. ESSER[2]
[1]*Department of Geology, The Colorado College, 14 E. Cache la Poudre, Colorado Springs, Colorado 80903, USA (e-mail: csiddoway@coloradocollege.edu)*
[2]*New Mexico Geochronological Research Laboratory, New Mexico Bureau of Mines and Mineral Resources, 801 Leroy Place, Socorro, NM 87801, USA*

Abstract: Intracontinental deformation occurred in West Antarctica during the final stages of plate convergence along the Cretaceous Gondwana margin. In western Marie Byrd Land, 115 Ma to 95 Ma A-type granitoids and mafic dykes record a change in plate kinematics. The magmatism typically is viewed as a record of extension leading to orthogonal break-up between New Zealand and Marie Byrd Land by *c.* 67 Ma. This paper presents new kinematic and $^{40}Ar/^{39}Ar$ age data for a mafic dyke array in the Ford Ranges, a region >1000 km^2 dominated by plutonic and metamorphic bedrock. The mean dyke trend of N16W corresponds to a maximum finite strain axis orientated N74E, highly oblique to the N58E-trending margin and to on-land crustal structures defined from airborne geophysics. $^{40}Ar/^{39}Ar$ emplacement ages for most dykes fall between 114 Ma and 97 Ma, coeval with emplacement of a gneiss dome at 101–96 Ma and with development of mylonitic shear zones at 100–95 Ma in coastal western Marie Byrd Land. The oblique orientation of maximum finite strain with respect to large faults, geophysical lineaments and the rifted margin of western Marie Byrd Land is consistent with transcurrent tectonics along this segment of the Gondwana margin at *c.* 100 Ma.

Continental extension occurred within the western Marie Byrd Land terrane (Fig. 1) during final stages of plate convergence along the Gondwana margin in West Antarctica–New Zealand. The event is recorded by *c.* 107 Ma mafic dykes in central Marie Byrd Land (Storey *et al.* 1999) and by *c.* 115–95 Ma A-type granite plutons (Weaver *et al.* 1992; 1994) overprinted by high strain zones having 101–94 Ma $^{40}Ar/^{39}Ar$ mineral cooling ages (Richard *et al.* 1994; Siddoway *et al.* 2004*a*) in the Ford Ranges of western Marie Byrd Land (Fig. 2). In the absence of regional kinematic data, magmatism and mid-crustal flow typically are interpreted in terms of pure shear extension orthogonal to the continental margin (e.g. Richard *et al.* 1994; Storey *et al.* 1999). A persistent problem for kinematic interpretation in the region is the comparative homogeneity of bedrock units, absence of dynamic fabrics in plutonic rocks, lack of exposure of large-scale faults or crustal-scale shear zones and the lack of precise age control upon mesoscopic brittle structures (Luyendyk *et al.* 2003; Siddoway *et al.* 2004*a*). Comprehensive structural analysis, including study of anisotropy of magnetic susceptibility (AMS) fabrics, has been conducted previously only on the singular exposures of middle crustal rocks that form the Fosdick Mountains migmatite dome (Siddoway *et al.* 2004*b*).

Mafic dykes present throughout the Ford Ranges offer the means to determine directly the regional finite strain ellipsoid during Cretaceous magmatism in the Ross Province of western Marie Byrd Land. This paper presents a geometrical analysis of the regional dyke array, together with $^{40}Ar/^{39}Ar$ age data that provide constraints on timing of dyke emplacement. The kinematic record from mafic dykes is considered together with kinematic information from brittle faults (Luyendyk *et al.* 2001; 2003) and ductile structures (Richard *et al.* 1994; Siddoway *et al.* 2004*b*) in the Ford Ranges, in order to develop a transcurrent model for Early Cretaceous tectonism along this segment of the Gondwana margin in Albian time.

Geological background

Marie Byrd Land in West Antarctica (Dalziel & Elliot 1982; Storey *et al.* 1988; Bradshaw *et al.* 1997) forms the northern flank of the West Antarctic rift system (Storey *et al.* 1999) and has geological affinities with New Zealand and northern Victoria Land (Ireland *et al.* 1994; Muir *et al.* 1994; Bradshaw *et al.* 1997). Pankhurst *et al.*

From: VAUGHAN, A. P. M., LEAT, P. T. & PANKHURST, R. J. (eds) 2005. *Terrane Processes at the Margins of Gondwana*. Geological Society, London, Special Publications, **246**, 417–438. 0305-8719/$15.00

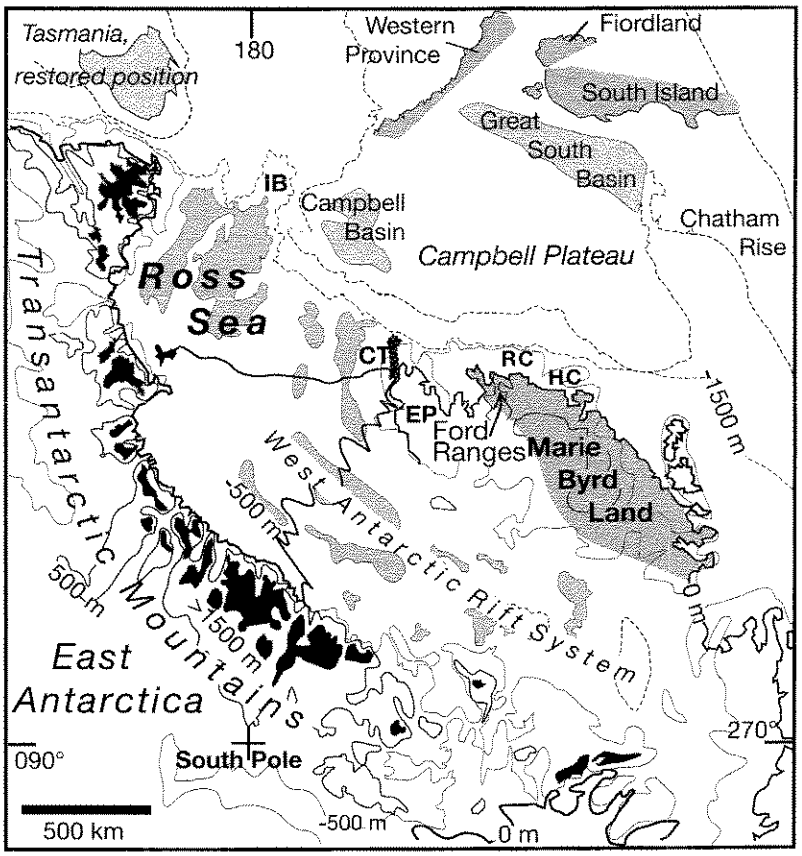

Fig. 1. Tectonic reconstruction of the Marie Byrd Land–New Zealand sector of the Cretaceous Gondwana margin at *c.* 100 Ma. The rifted margin corresponds to the *c.* 1500 m contour (dashed-line pattern), which defines a linear to curvilinear trace for a distance >1500 km bordering the Ross Sea and western Marie Byrd Land. The margin trends N58E along Ruppert Coast, changing to N75E along Hobbs Coast. The dramatic increase in depth along a linear or small circle trace, together with the very close fit with the –1500 m contour for Campbell Plateau, suggest structural controls upon the rifted margin. CT, Campbell Trough; EP, Edward VII Peninsula; HC, Hobbs Coast; IB, Iselin Bank; RC, Ruppert Coast. Based on Sutherland (1999).

(1998) distinguish two provinces within Marie Byrd Land; the eastern Amundsen Province of arc character and the western Ross Province of continental affinity. Mafic dykes pervade both provinces; however, the prevalent orientation in the Ross Province (this paper) differs from that in the Amundsen province (Storey *et al.* 1999). Storey *et al.* (1999) determined that the Amundsen Province array exposed along Ruppert Coast (Fig. 1) is orientated N80W, subparallel to the coast except where dykes intrude pre-existing N–S structures.

The Palaeozoic Ross Province, the focus of this study, comprises folded, low greenschist-grade metagreywackes of the Swanson Formation (Bradshaw *et al.* 1983), intruded by Ford Granodiorite (I-type; Weaver *et al.* 1991; Pankhurst *et al.* 1998) (Fig. 2). Swanson Formation represents detritus shed from the early Palaeozoic Ross Orogen (Ireland *et al.* 1994; Pankhurst *et al.* 1998). In middle Cretaceous time, A-type granitoids collectively known as Byrd Coast Granite were emplaced; these have a geochemical character indicative of a continental extensional province (Weaver *et al.* 1992; 1994; Adams *et al.* 1995). Further evidence of tectonic divergence comes from a discordance in Cretaceous palaeomagnetic poles between East Antarctica and Marie Byrd Land (DiVenere *et al.* 1994; Luyendyk *et al.* 1996); gravity data that delimit a 8–9 km contrast in crustal thickness between the Ross

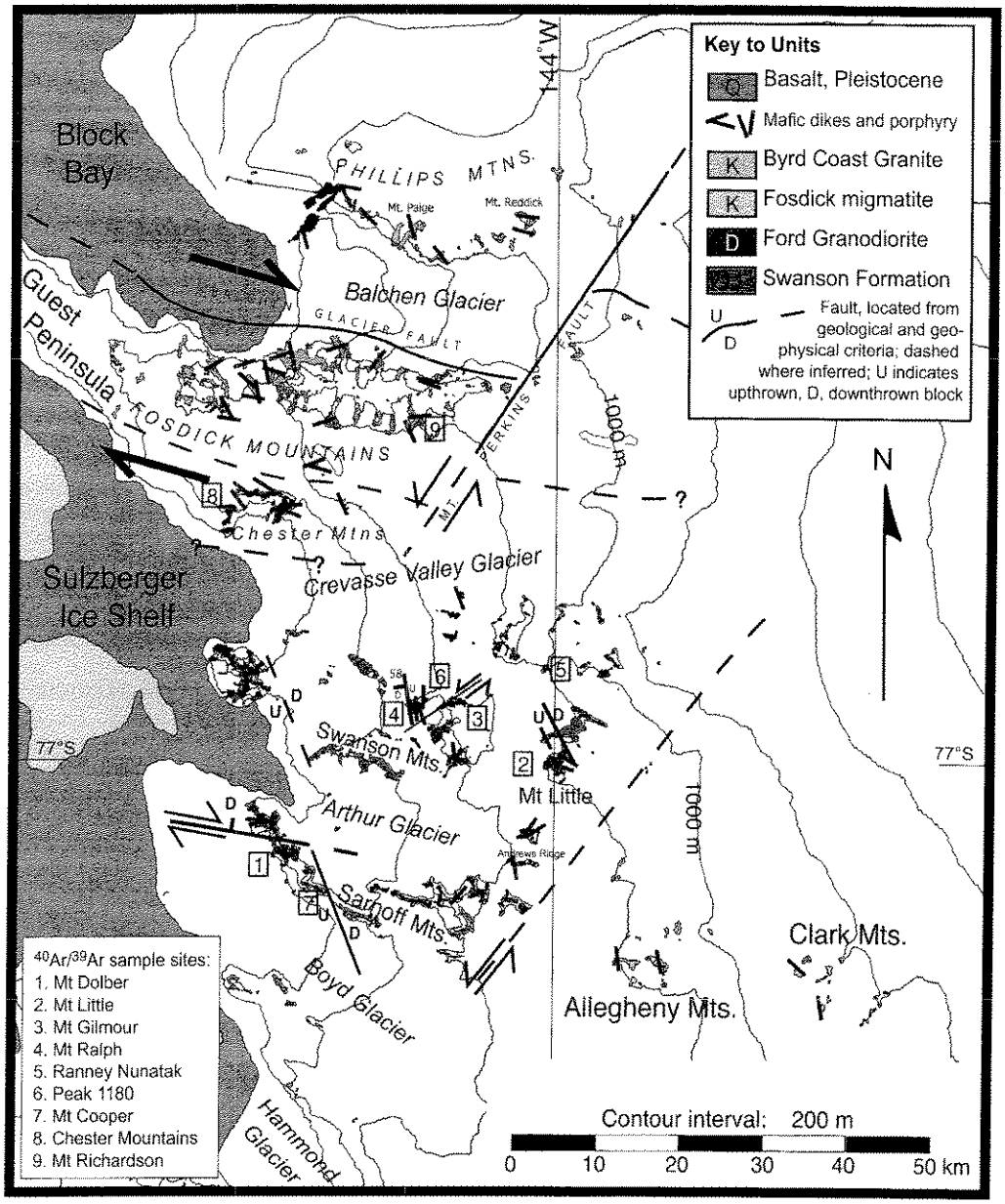

Fig. 2. Geological map of the Ford Ranges, western Marie Byrd Land. Location and trend of mafic dykes are shown with orange bars generally, and with brown bars in the Fosdick Mountains. Sample sites for dykes used for $^{40}Ar/^{39}Ar$ age determination are numbered. The Ford Ranges comprise early Palaeozoic greywacke and argillite of the Swanson Formation intruded by Devonian Ford Granodiorite and Cretaceous Byrd Coast Granite. These formations are, in turn, intruded by mafic dykes; felsic dykes intrude the Byrd Coast Granite only. Inferred faults correspond with contrasts in metamorphic grade between ranges, geophysical lineaments or boundaries, and zones of penetrative brittle deformation.

Sea and central Marie Byrd Land (Luyendyk *et al.* 2003); Late Cretaceous mineral cooling and apatite fission track ages throughout the Ross Province (Richard *et al.* 1994; Lisker & Olesch 1998; Pankhurst *et al.* 1998); and, in the northern Ford Ranges, a migmatite-cored gneiss dome in the Fosdick Mountains, emplaced and cooled rapidly between 105 Ma and 94 Ma (Richard *et al.* 1994). Textural and petrological evidence for rapid decompression, together with the thermal history, indicate that diapirism played a role in dome emplacement (Siddoway *et al.* 2004*b*).

Offshore, high-angle normal faults have been imaged by marine seismic survey and, along one of them, samples of mylonitized Byrd Coast Granite were recovered by dredge (Luyendyk *et al.* 2001). The mylonitic gneisses formed in a shear zone at *c.* 98 Ma and underwent rapid cooling as a consequence of tectonic exhumation (Siddoway *et al.* 2004*a*). On land, field investigation and analysis of airborne geophysics data identify a regional fault pattern of dextral and sinistral faults in a conjugate geometry (Fig. 2; Luyendyk *et al.* 2003). In this region dominated by isotropic plutonic rocks, the primary means to obtain kinematic data directly is through analysis of mesoscopic-scale brittle structures including minor faults, shear fractures and mafic dykes that cut Byrd Coast Granite and older units (Luyendyk *et al.* 2003). The paucity of reliable geological markers to quantify fault offsets or provide age control make the mafic dykes of great value for strain studies, using the assumption that dykes emplaced in previously unfractured rock propagate in a plane normal to the maximum principal finite strain (i.e. least compressive stress direction, Tsunakawa 1983; Best 1988).

Recent efforts to integrate findings from brittle kinematic studies throughout the Ford Ranges (Luyendyk *et al.* 2003) with results from the Fosdick Mountains dome (Richard *et al.* 1994) found a transcurrent model to be most compatible with regional structural patterns (Siddoway *et al.* 2004*b*). The mafic dykes throughout the Ford Ranges provide a direct means to determine age and kinematic setting for the time of their emplacement and, consequently, to determine whether their kinematics are consistent with transtension (e.g. Luyendyk *et al.* 1992, fig. 6) or orthogonal extension (e.g. Storey *et al.* 1999) along this sector of the Cretaceous Gondwana margin.

The Ford Ranges dyke array: description and structural geometry

Present in both the Carboniferous Ford Granodiorite and Cretaceous Byrd Coast Granite, mafic dykes of the Ford Ranges are typically 2–4 m thick and have steeply dipping, planar contacts with host rock (Figs 3a, b; Table 1). They have great lateral extent along-strike; however, they are widely spaced at 15 m to 1500 m. Thicknesses range from 0.5 m to 14 m. The dykes typically are dolerite, with fine-grained plagioclase laths within an aphanitic groundmass of anhedral to subhedral hornblende and pyroxene. Several dykes are plagioclase- and pyroxene-porphyritic. One unusual dyke contains large pyroxene phenocrysts up to 3 cm in length; the rock is vesicular and developed columnar joints (Fig. 3c). Petrographic study shows that typical groundmass consists of varying proportions of augite, amphibole, biotite and plagioclase. Hornblende is commonly zoned, with some alteration to actinolite: Epidote, chlorite or calcite may be present, particularly in dykes with sheared margins. Pyrite and non-magnetic opaque grains are abundant accessory minerals and accessory apatite is present in some samples.

Ford Ranges dyke orientations, Fosdick Mountains excluded, are summarized in Figure 4. Figures 4a and b provide a comparison of data from the northern versus southern Ford Ranges as a means to assess regional variations. Fosdick Mountains data are considered separately (Fig. 5) because migmatite gneisses representative of middle crust (Siddoway *et al.* 2004*b*) are exposed in that range. All structural attitudes were measured with respect to geographical north at outcrops throughout the Ford Ranges between 142° W and 146° W longitude (Fig. 2).

A prevalent mafic dyke array in the southern Ford Ranges is orientated N16W with subvertical dips (Fig. 4a), suggesting a predominant ENE–WSW stretching direction at the time of dyke emplacement. This population is also present in the northern Ford Ranges; however, a conjugate dyke array distinguished by moderate dips to NE and SW (Fig. 4b) is also present. Seven of thirteen of the NE-striking dykes intrude brittle faults with sinistral sense, low-raking striae; thus, it is probable that these dykes intruded upon contemporaneous or pre-existing structures. The eastern Phillips Mountains (Fig. 2) host a suite of felsic porphyry dykes cutting Byrd Coast Granite and these steeply dipping felsic dykes strike NNW–SSE (Fig. 4c), consistent with the prevalent mafic dyke orientation for the region. The small

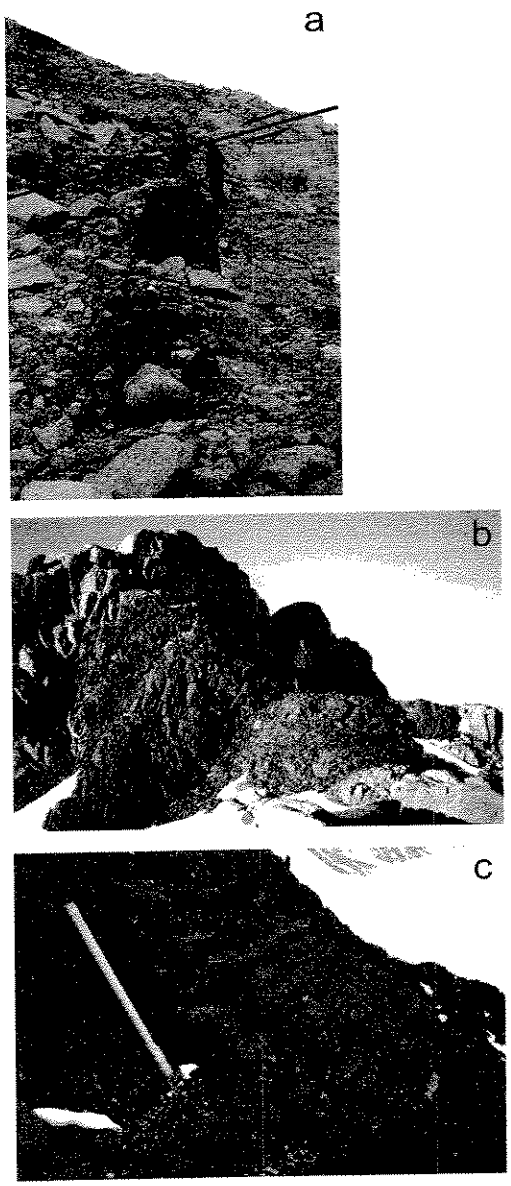

Fig. 3. Outcrop photos illustrating dyke geometry and extent. (**a**) Dyke of width 2 m is orientated 340/89 NE. The dyke is cut by a NE-striking brittle fault with low-raking striae; the offset is 5 m in a sinistral sense. $^{40}Ar/^{39}Ar$ sample 9N23-4 was collected from this dyke at Mt Ralph. (**b**) Large, steep dyke at Andrews Ridge orientated 000/81 E; thickness is 4 m (not analysed). (**c**) Wide dyke of columnar-jointed, vesicular plagioclase basalt, orientated 355/82 E. $^{40}Ar/^{39}Ar$ sample L9N17-1 was collected from this site at Mt Little.

dataset in Figure 4d summarizes the foliation and lineation fabrics of a rare exposure of mylonitized Ford Granodiorite at Mt Cooper in the Sarnoff Range. The mylonite data are included here because a mylonite gneiss sample investigated using $^{40}Ar/^{39}Ar$ thermochronology yields similar kinematic and age results as mafic dykes. The $^{40}Ar/^{39}Ar$ age for dynamically recrystallized biotite in the normal-sense shear zone, reported below, is 97 Ma, concordant within error with the 96 Ma ages of the youngest dykes. Finally, Figure 4e shows the orientations of mafic dykes that intrude Byrd Coast granite plutons and, as such, are sure to be Albian aged or younger.

Evident in Figure 5, dyke geometries in the Fosdick Mountains contrast with those elsewhere. The mean orientation of 102/80 SW is nearly orthogonal to the dyke trends in the broader Ford Ranges summarized in Figure 4.

$^{40}Ar/^{39}Ar$ age investigation

Mafic dykes and host rocks from 11 sites distributed widely within the Ford Granodiorite (Fig. 2) were sampled for $^{40}Ar/^{39}Ar$ age dating. The aphanitic texture of the dyke rock necessitated the use of groundmass concentrate separates as the phase to be dated. Biotite and muscovite mineral separates were obtained from four host-rock samples, including sample 9D7-4 from a narrow mylonitic shear zone at Mt Cooper. Samples were analysed by the resistance-furnace incremental-heating age spectrum method at the New Mexico Geochronology Research Laboratory (NMGRL). Analytical methods are summarized in Table 2.

The nine groundmass concentrate samples yield slightly to severely discordant age spectra (Fig. 6; Table 3). Five of the samples (9D9-1, 9N17-2, 9N23-4, 9N25-8 and L9N16-2) yield spectra with initial anomalously young apparent ages at the lowest temperature steps, followed by monotonically increasing ages at the intermediate to highest temperature steps. For these samples, high K–Ca ratios generally coincide with older apparent ages. For most samples, isotope correlation diagrams (also known as inverse isochron diagrams) yield trapped $^{40}Ar/^{36}Ar$ ratios equivalent to present-day atmosphere (295.5) and ages are analytically indistinguishable from their respective spectrum-weighted mean ages.

For most of the groundmass concentrate samples, rising age spectra and correspondence of initial young ages to the lowest radiogenic yields (Figs 6, 8) are attributed to alteration of finer-grained groundmass, with non-diffusive

Table 1. Summary of field relationships for dykes used for $^{40}Ar/^{39}Ar$ study

Location, site #, and strike/dip of margin	Schematic diagram	Sample number and description	Age and cross-cutting relationships
Mt Little 143°50′ W 77°00′ S Site 2 in Figure 2 300/90	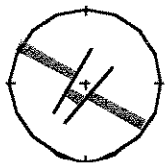	L9N16-2 Dolerite with acicular plagioclase in fine-grained groundmass.	142.0 ± 0.7 Ma Cut by NE faults with strike-slip striae.
Mt Little 143°50′ W 76°58′ S Site 2 in Figure 2 Various	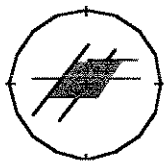	L9N17-1 Vesicular basalt intrusion with columnar joints. Pyroxenes up to 10 cm; fine-grained plagioclase laths.	96.38 ± 3.54 Ma Intrudes E–W and NE–SW fractures. It is not cut by faults.
Mt Gilmore 144°35′ W 76°56′ S Site 3 in Figure 2 241/80	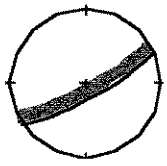	9N20-1 Fine-grained light grey dolerite hornblende and pyroxene; contains resorbed Qz reaching 8 mm and xenoliths with reaction rims.	102.2 ± 1.7 Ma Intrudes brittle fault with shallow fault striae.
Mt Ralph 144°31′ W76°58′ S Site 4 in Figure 2 340/89		9N23-4 Medium-grained dolerite with augite >1 mm. Px replaced by Hbl. Contains granite xenoliths.	274.2 ± 13.4 Ma
Ranney Nunatak 143°55′ W76°53′ S Site 5 in Figure 2 305/90	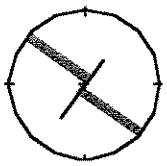	9N25-8 Very fine-grained dolerite with plagioclase, hornblende ± pyroxene.	136.9 ± 2.6 Ma Cut by high angle fault with right separation.
Peak 1180 144°22′ W 76°56′ S Site 6 in Figure 2 342/86	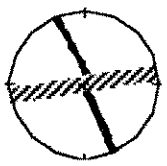	L9N27-1 Fine-grained dolerite with biotite after hornblende. Contains granitic xenoliths.	110.6 ± 3.1 Ma Dyke is cut by a chloritic shear zone, shown with cross-hatch pattern.
Mt Dolber 145°28′ W 77°07′ S Site 1 in Figure 2 225/75	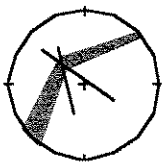	9D9-1 Fine-grained dolerite with biotite after hornblende.	96.15 ± 2.08 Ma

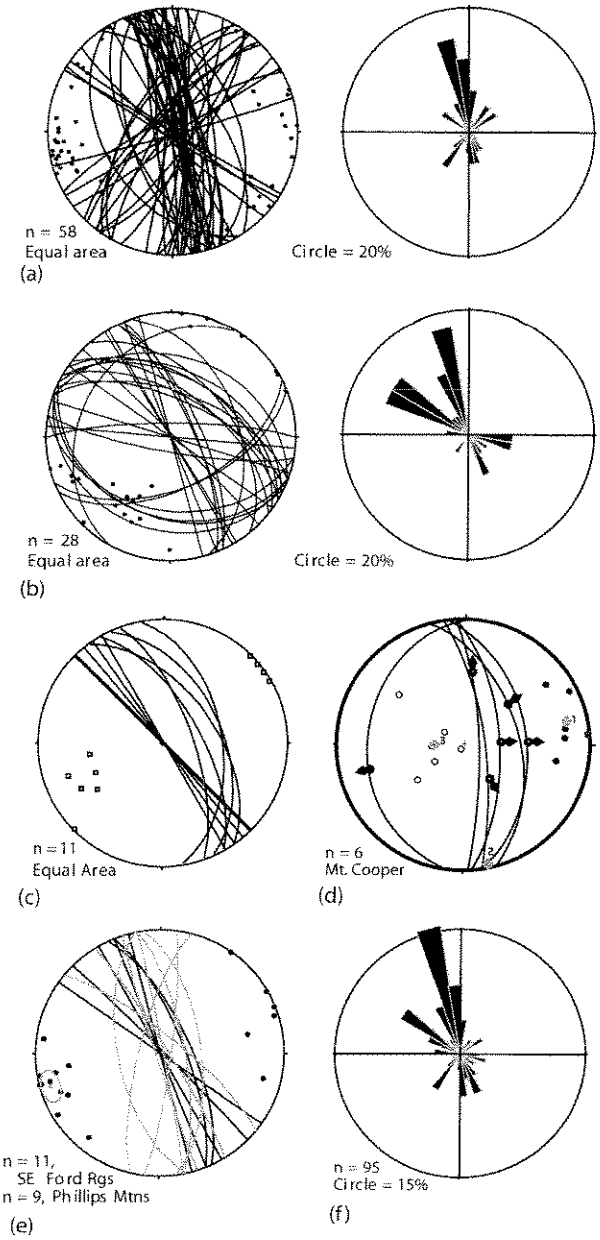

Fig. 4. Structural data for dykes and a shear zone that cut granitoids of the Ford Ranges. Attitude of dyke margin or of mylonitic foliation are summarized on equal-area stereographic diagrams. The Crevasse Valley Glacier is used to subdivide the Ford Ranges in to southern and northern regions for purposes of structural analysis, to assess regional variations. For locations, refer to Figure 2. Diagrams in this and subsequent figures were prepared using Stereonet v. 6.2.X by R. W. Allmendinger. (**a**) Southern Ford Ranges stereoplot and rose diagram; (**b**) northern Ford Ranges stereoplot and rose diagram, exclusive of Fosdick migmatite gneiss dome (see Fig. 5); (**c**) summary diagram of felsic porphyry dykes intruding Byrd Coast Granite, Phillips Mountains; (**d**) summary diagram of mylonitic foliation and mineral stretching lineation within narrow shear zones at Mt Cooper (Fig. 2). The $^{40}Ar/^{39}Ar$ biotite age of 97 Ma for a mylonite sample is presented in Table 2. (**e**) Orientations of mafic dykes that cut Byrd Coast Granite plutons; (**f**) summary rose diagram for the Ford Ranges showing the dominant regional dyke orientation of N16 W.

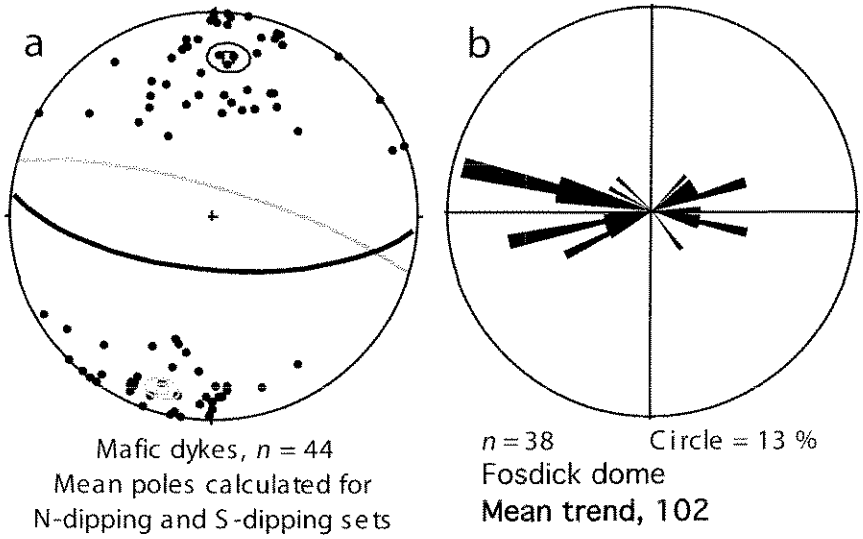

Fig. 5. Equal-area stereographic diagrams for mafic dykes that cut foliation and folds in the Fosdick Mountains gneiss dome. The attitudes of dyke margins are summarized. The dykes trend WNW–ESE, with steep dips to both NNE and SSW. The Fosdicks dyke array is nearly orthogonal to systematic dykes of the broader Ford Ranges.

argon loss from matrix phases (e.g. Foland *et al.* 1993). Complex heating behaviour for dyke samples was also noted by Richard *et al.* (1994). Textural evidence of breakdown of pyroxene and hornblende to retrograde products, exacerbated where faults overprint dykes (Table 1), is a sign of this alteration.

Due to the effects of alteration, the preferred isochron or plateau ages within the range 142–97 Ma are considered to be minimum ages for most samples. Where MSWD analysis (cf. Mahon 1996) on each plateau segment or inverse isochron indicates that the single population criterion was not fulfilled at 95% probability, the errors on the weighted mean age or isochron age are adjusted (Tables 2–4). Although the $^{40}Ar/^{39}Ar$ age determinations are not of high quality due to minor amounts of alteration, the results nonetheless establish the time of emplacement of most dykes to be Albian, consistent with the observation that the dykes cut 102–95 Ma age Byrd Coast Granite and older rocks. Two dykes give older ages of 137 Ma and 146 Ma. Moreover, all of the dated dykes form part of a systematic structural array with a mean strike of N16W.

Biotite or muscovite mineral separates were prepared from plutonic host rock bordering mafic dykes at four sites (Fig. 7), together with a biotite separate for a sample from a 3 m wide mylonite shear zone (Fig. 8) in the southern Ford Ranges. The spectra for each mica are relatively well-behaved with only minor amounts of $^{40}Ar^*$ loss in the lowest temperature steps, probably the result of minor chloritization. The weighted mean of the flattest portion of each biotite and muscovite age spectrum is interpreted as the crystallization age of the sample. In the case of sample 9D7-4, the weighted mean (96.92 ± 0.34 Ma) is interpreted as the recrystallization age of the biotite within the mylonite zone.

A similar age comes from an undeformed mafic dyke in the Fosdick Mountains gneiss dome, investigated in a previous study (Richard *et al.* 1994). $^{40}Ar/^{39}Ar$ hornblende results yielded concordant plateau and isochron ages of 97.8 ± 0.1 Ma and 96.4 ± 1.1 Ma (Table 2). A complex hornblende age spectra from a Chester Mountains sample (Fig. 2; Table 2) gave apparent ages varying irregularly between 148 Ma and 102 Ma, and a total gas age of 122 Ma. The complexity in $^{40}Ar/^{39}Ar$ results is attributable to complexly zoned hornblende with actinolitic rims (Richard *et al.* 1994).

$^{40}Ar/^{39}Ar$ weighted mean ages for biotite and muscovite separated from dyke wall rock samples range from 351 ± 2 Ma to 342.4 ± 1 Ma (Table 2; Fig. 7), a confirmation that the plutonic rock hosting the mafic dykes is Ford Granodiorite (cf. Pankhurst *et al.* 1998).

Table 2. Summary of $^{40}Ar/^{39}Ar$ age determinations for Ford Ranges mafic dykes

Sample number	Sample locality	Site on Figure 2	Preferred age*	*n*	%^{39}Ar	MSWD	K–Ca	Age	±2σ
Ages determined from groundmass concentrates									
9D9-1	Mt Dolber, Sarnoff Range	1	isochron	8	.....	50.3	.....	96.15	2.08‡
9N17-1	Mt Little, west central Ford Ranges	2	isochron	9	.....	68.7‡	.....	96.38	3.54‡
9N17-3	Mt Little, west central Ford Ranges	2	isochron	9	.....	109‡	.....	40.82	2.31‡
9N20-1	Mt Gilmour, Denfield Mountains	3	plateau	3	71.6	20.1‡	4.20	102.2	1.7‡
9N20-2	Mt Gilmour, Denfield Mountains	3	isochron	9	.....	209‡	.....	113.5	5.8‡
9N23-4	Mt Ralph, Denfield Mountains	4	isochron	5	.....	0.8	.....	274.2	13.4‡
9N25-8	Ranney Nunatak, Gutenko Nunataks	5	isochron	8	.....	21.4‡	.....	136.9	2.6‡
9N27-1	Peak x1180, Denfield Mountains	6	isochron	7	.....	181‡	.....	108.8	7.0‡
L9N16-2	Mt Little, west central Ford Ranges	2	plateau	6	88.1	6.1‡	0.83	142.0	0.7‡
Ages determined from mineral separates									
9D7-4	Mt Cooper, Sarnoff Range	7	plateau, bt	9	93.9	3.4‡	21.6	96.92	0.34‡
L9N15-1	Mt Little, west central Ford Ranges	2	plateau, mu	7	94.7	2.1	368.7	342.4	1.0‡
L9N17-2	Mt Little, west central Ford Ranges	2	plateau, mu	8	92.6	0.8	28.4	348.2	0.9‡
L9N17-3	Mt Little, west central Ford Ranges	2	plateau, mu	8	93.3	3.2‡	21.6	347.3	1.2‡
L9N17-3	Mt Little, west central Ford Ranges	2	plateau, bt	3	43.3	8.0‡	12.2	350.8	2.1‡
Chester-2	Chester Mountains	8	total gas	Sample details are provided in				122	
Mutel-1	Fosdick Mountains	9	plateau	Richard *et al.* (1994)				96.4	1.1

* Isochron ages, $^{40}Ar/^{36}Ar_i$ and MSWD values calculated from regression results obtained by the methods of York (1969). Decay constants and isotopic abundances follow Steiger & Jäger (1977).

‡ Two-σ errors. All final errors are reported at ±2σ, unless otherwise noted. Weighted mean error is calculated using the method of Taylor (1982).

‡ Mean standard weighted deviation (MSWD) outside 95% confidence interval. Weighted mean age is calculated by weighting each age analysis by the inverse of the variance. MSWD values are calculated for $n - 1$ degrees of freedom for plateau and preferred ages.

Sample preparation: Groundmass concentrates, biotites and muscovites separated using standard techniques of crushing, sieving, magnetic separation and hand-picking. Groundmass concentrates were packaged and irradiated in machined Al discs for 7 hours in D-3 position, Texas A&M University Research Reactor. Biotite and muscovite mineral separates were packaged and irradiated in machined Al discs for 24 hours in L67 position, Ford Research Reactor, University of Michigan.

The neutron flux monitor used is Fish Canyon Tuff sanidine (FC-1) of assigned age = 27.84 Ma (Deino & Potts 1990) relative to standard Mmhb-1 at 520.4 Ma (Samson & Alexander 1987). The Richard *et al.* (1994) horneblende ages are recalculated using the 27.84 flux monitor age, for conformity with NMGRL data.

Sample procedures: The instrument used is a Mass Analyzer Products 215-50 mass spectrometer on-line with automated all-metal extraction system. All samples were step-heated in Mo double-vacuum resistance furnace. Duration of heating is 6–8 minutes. Reactive gases were removed with 2 SAES GP-50 getters, one operated at *c.* 450 °C and one at 20 °C, during the 6-minute reaction. Gases were also exposed to a W filament operated at *c.* 2000 °C.

Analytical parameters: Electron multiplier sensitivity is averaged 3.06×10^{-16} moles pA^{-1} for samples analysed by the laser. The total system blank and background for the step-heated samples averaged 1040, 2.7, 1.3, 1.1, 3.4×10^{-17} moles. J-factors were determined to a precision of ± 0.1% by CO_2 laser-fusion of four single crystals from each of four or six radial positions around the irradiation tray. Correction factors for interfering nuclear reactions were determined using K-glass and CaF_2 and are as follows:

Texas A&M: $(^{40}Ar/^{39}Ar)K = 0.0002 \pm 0.0003$
$(^{36}Ar/^{37}Ar)Ca = 0.00028 \pm 0.00001$
$(^{39}Ar/^{37}Ar)Ca = 0.00089 \pm 0.00003$
Michigan: $(^{40}Ar/^{39}Ar)K = 0.0262 \pm 0.0003$
$(^{36}Ar/^{37}Ar)Ca = 0.00028 \pm 0.00001$
$(^{39}Ar/^{37}Ar)Ca = 0.00078 \pm 0.00003$

Discussion

Throughout most of the Ford Ranges, mafic dykes record regional ENE–WSW stretching orthogonal to dyke margins (Fig. 4f). The observation that dykes cutting Byrd Coast Granite of 102–95 Ma age (Fig. 4c) and dykes emplaced within older rocks (Figs 4a, b) are co-parallel makes it unlikely that dykes commonly intruded upon pre-existing fractures unrelated to the middle Cretaceous state of stress (e.g. Best 1988). The exception is NE-striking, moderately steeply dipping dykes. These intrude brittle faults with shallowly plunging striae, an indication that dykes exploited pre-existing structures.

The mesoscopic normal-sense mylonitic shear

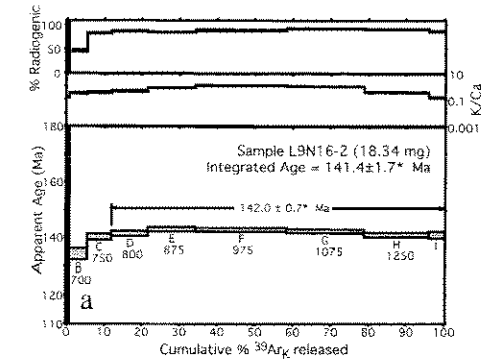
% Radiogenic
K/Ca
Apparent Age (Ma)
Sample L9N16-2 (18.34 mg)
Integrated Age = 141.4±1.7* Ma
142.0 ± 0.7* Ma
Cumulative % $^{39}Ar_K$ released
a

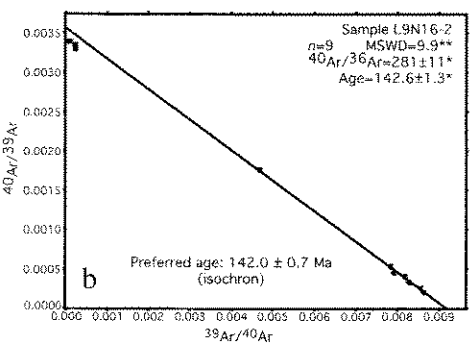
Sample L9N16-2
n=9 MSWD=9.9**
$^{40}Ar/^{36}Ar$=281±11*
Age=142.6±1.3*
$^{40}Ar/^{39}Ar$
Preferred age: 142.0 ± 0.7 Ma
(isochron)
$^{39}Ar/^{40}Ar$
b

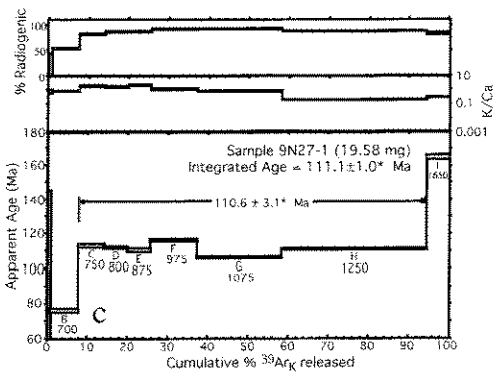
% Radiogenic
K/Ca
Apparent Age (Ma)
Sample 9N27-1 (19.58 mg)
Integrated Age = 111.1±1.0* Ma
110.6 ± 3.1* Ma
Cumulative % $^{39}Ar_K$ released
c

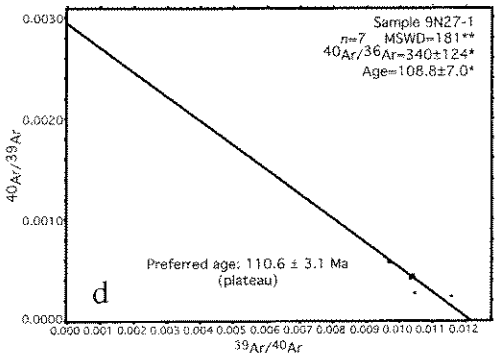
Sample 9N27-1
n=7 MSWD=181**
$^{40}Ar/^{36}Ar$=340±124*
Age=108.8±7.0*
$^{40}Ar/^{39}Ar$
Preferred age: 110.6 ± 3.1 Ma
(plateau)
$^{39}Ar/^{40}Ar$
d

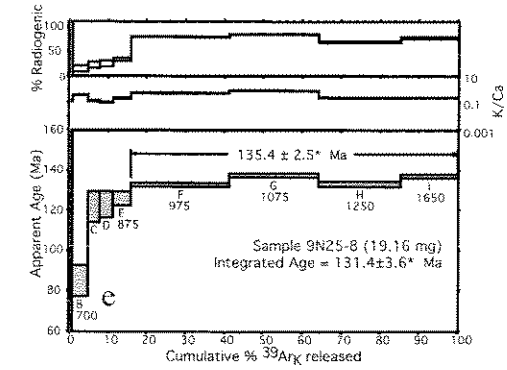
% Radiogenic
K/Ca
Apparent Age (Ma)
135.4 ± 2.5* Ma
Sample 9N25-8 (19.16 mg)
Integrated Age = 131.4±3.6* Ma
Cumulative % $^{39}Ar_K$ released
e

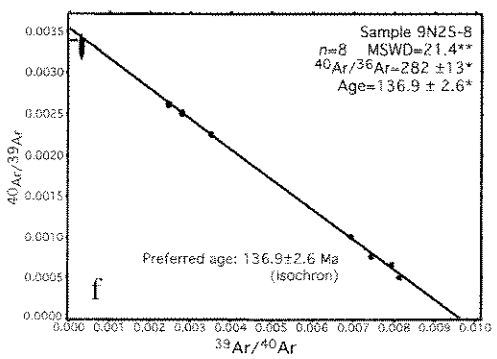
Sample 9N25-8
n=8 MSWD=21.4**
$^{40}Ar/^{36}Ar$=282 ±13*
Age=136.9 ± 2.6*
$^{40}Ar/^{39}Ar$
Preferred age: 136.9±2.6 Ma
(isochron)
$^{39}Ar/^{40}Ar$
f

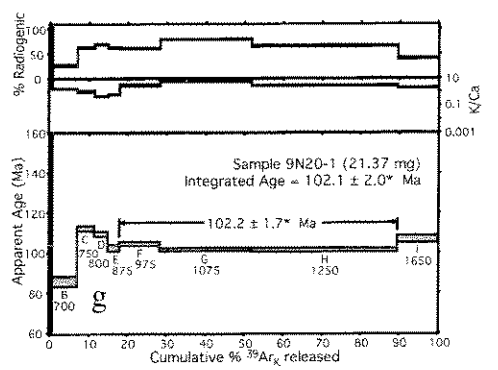
% Radiogenic
K/Ca
Apparent Age (Ma)
Sample 9N20-1 (21.37 mg)
Integrated Age = 102.1 ± 2.0* Ma
102.2 ± 1.7* Ma
Cumulative % $^{39}Ar_K$ released
g

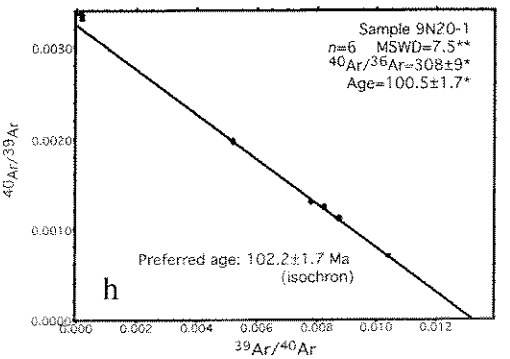
Sample 9N20-1
n=6 MSWD=7.5**
$^{40}Ar/^{36}Ar$=308±9*
Age=100.5±1.7*
$^{40}Ar/^{39}Ar$
Preferred age: 102.2±1.7 Ma
(isochron)
$^{39}Ar/^{40}Ar$
h

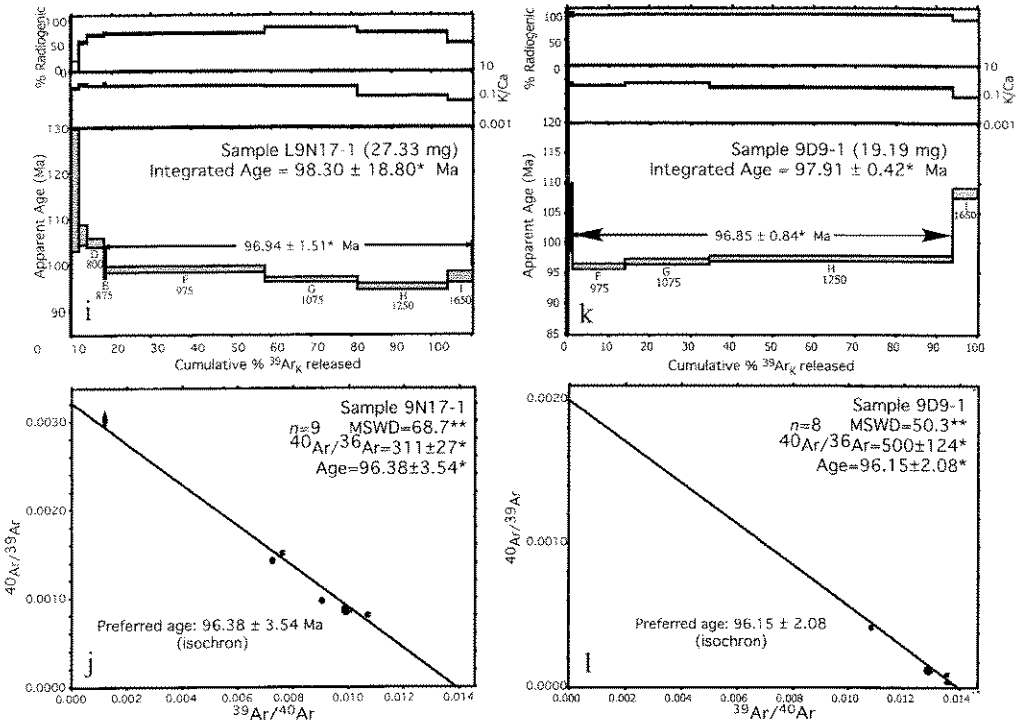

Fig. 6. $^{40}Ar/^{39}Ar$ age spectra and inverse isochron diagrams for representative groundmass concentrate separates for dolerite dykes. Each of the nine groundmass concentrates yielded slightly to severely discordant age spectra; thus both plateaux or weighted mean ages and inverse isochron ages are calculated. For most samples, the inverse isochron ages are analytically identical to plateau ages. The preferred age for each sample is noted here and summarized again in Figure 9. Diagrams for samples 9N17-3, 9N20-2 and 9N23-4 are not shown. The samples produced very disturbed spectra indicative of extensive alteration, have unacceptable error in 2σ and yield results of overall low quality. (**a, b**) Sample L9N16-2; (**c, d**) sample L9N27-1; (**e, f**) sample L9N25-8; (**g, h**) sample L9N20-1; (**i, j**) sample L9N17-1; (**k, l**) sample 9D9-1. All errors are reported at 2σ.

zones at Mt Cooper (Fig. 2) record stretching orientated *c.* N75E (Fig. 4d) at 96.92 ± 0.34 Ma, according to the $^{40}Ar/^{39}Ar$ age on biotite (Fig. 6) forming part of the mylonitic fabric. Within the Fosdick gneiss dome, folds, ductile fabrics and AMS strain axes for migmatite gneisses indicate a finite strain axis orientated N65E during high temperature metamorphism and dome emplacement (Siddoway *et al.* 2004*b*). The stretching direction is oblique to the N80W-trending Balchen Glacier Fault that bounds the dome on its north side (Fig. 2). The consistent results from brittle and ductile criteria from differing levels of crustal exposure provide firm evidence for a NE to ENE maximum finite strain direction across the Ford Ranges at the time of dyke emplacement. The orientation of felsic and mafic dykes (Figs 4c, e) cross-cutting Cretaceous Byrd Coast Granite plutons in the Phillips, Clark, Allegheny Mountains (Fig. 2) help support this interpretation.

The timing of regional dyke emplacement and NE to ENE stretching is well constrained by cross-cutting relationships of the parallel array of dykes that intrude both Byrd Coast Granite and Ford Granodiorite (Figs 4e, a, respectively) together with the $^{40}Ar/^{39}Ar$ results for Ford Ranges dykes (Figs 6, 9). The geological and thermochronological data show that the prevalent dyke ages are Aptian, with two older results in the latest Jurassic and earliest Cretaceous. The structural data presented here provide a clear record of the regional kinematic setting at that time and prove that the *c.* N70E regional stretching direction was not orthogonal to the (present-day) rifted margin of western Marie Byrd Land as has been thought previously (e.g. Richard *et al.*

Table 3. Results of $^{40}Ar/^{39}Ar$ analysis of groundmass concentrate separates for mafic dyke samples

ID	T (°C)	$^{40}Ar/^{39}Ar$	$^{37}Ar/^{39}Ar$	$^{36}Ar/^{39}Ar$ $\times 10^{-3}$r	$^{39}Ar_K$ $\times 10^{-16}$ mol	K–Ca	$^{40}Ar^*$ (%)	^{39}Ar (%)	Age (Ma)	±1σ (Ma)
9D9-1, E6:130, 19.10 mg whole rock, J = 0.00076235 ± 0.10%, NM-130, Lab# = 51769-02										
A √	*625*	*192.7*	*0.0697*	*703*	*–0.021*	*7.3*	*–7.8*	*0.0*	*–20.8*	*131.2*
B √	*700*	*213.7*	*1.838*	*480*	*0.417*	*0.28*	*33.7*	*0.2*	*96.5*	*6.7*
C √	*750*	*69.17*	*0.0000*	*1119*	*–0.001*	—	—	*0.2*	—	—
D √	*800*	*77.55*	*1.139*	*9.380*	*1.27*	*0.45*	*96.5*	*1.0*	*100.25*	*0.78*
E √	*875*	*80.13*	*0.8915*	*4.026*	*0.429*	*0.57*	*98.6*	*1.2*	*105.6*	*2.2*
F	975	73.51	1.255	6.467	22.0	0.41	97.5	13.8	96.11	0.21
G	1075	72.97	0.7900	2.360	35.9	0.65	99.1	34.4	96.91	0.20
H	1250	73.45	1.665	2.889	104.0	0.31	99.0	94.0	97.50	0.21
I √	*1650*	*91.84*	*7.368*	*39.77*	*10.5*	*0.069*	*87.9*	*100.0*	*108.40*	*0.37*
total gas age			$n = 9$		174.5	0.38			97.91	0.42*
plateau	MSWD = 11.1†		$n = 3$	steps F–H	161.9	0.40		92.8	96.85	0.84*
isochron	MSWD = 50.33†		$n = 8$			$^{40}Ar/^{36}Ar = 500 \pm 124$*			**96.15**	**2.08***
9N17-1, G1:130, 27.33 mg whole rock, J = 0.00075944 ± 0.10%, NM-130, Lab# = 51779-01										
A √	*625*	—	*0.0000*	—	*0.160*	—	*1.3*	*0.1*	—	—
B √	*700*	*833.9*	*0.7719*	*2525*	*4.25*	*0.66*	*10.5*	*1.9*	*116.4*	*6.6*
C √	*750*	*138.1*	*0.4424*	*196.1*	*4.48*	*1.2*	*58.0*	*3.8*	*106.6*	*1.0*
D √	*800*	*110.4*	*0.5426*	*107.1*	*9.65*	*0.94*	*71.4*	*8.0*	*104.94*	*0.44*
E √	*875*	*101.0*	*0.4202*	*87.01*	*0.945*	*1.2*	*74.6*	*8.4*	*100.4*	*1.6*
F	975	99.00	0.5203	83.74	92.5	0.98	75.0	48.3	99.07	0.32
G	1075	84.29	0.5945	39.81	53.5	0.86	86.1	71.4	96.84	0.22
H	1250	93.18	2.873	75.24	52.1	0.18	76.4	93.9	95.22	0.29
I	1650	130.7	6.574	198.7	14.1	0.078	55.5	100.0	97.29	0.56
total gas age			$n = 9$		231.7	0.71			98.30	18.80*
plateau	MSWD = 26.9†		$n = 4$	steps F–I	212.2	0.69		91.6	96.94	1.51*
isochron	MSWD = 68.7†		$n = 9$			$^{40}Ar/^{36}Ar = 311 \pm 27$*			**96.38**	**3.54***
9N17-3, E5:130, 19.86 mg whole rock, J = 0.000761894 ± 0.10%, NM-130, Lab# = 51768-01										
A √	*625*	—	*0.0000*	*55851*	*0.011*	—	*–1.6*	*0.0*	—	—
B √	*700*	*251.2*	*1.527*	*782.1*	*0.857*	*0.33*	*8.0*	*1.2*	*27.6*	*4.4*
C √	*750*	*84.89*	*0.4943*	*230.4*	*2.95*	*1.0*	*19.8*	*5.2*	*23.0*	*1.1*
D √	*800*	*199.8*	*2.513*	*602.2*	*3.22*	*0.20*	*11.0*	*9.6*	*30.1*	*1.9*
E √	*875*	*56.59*	*0.8472*	*109.8*	*3.30*	*0.60*	*42.8*	*14.2*	*33.00*	*0.70*
F √	*975*	*34.52*	*0.3844*	*23.07*	*20.8*	*1.3*	*80.3*	*42.6*	*37.74*	*0.15*
G	1075	38.36	0.3737	26.78	16.1	1.4	79.5	64.6	41.43	0.16
H	1250	40.69	1.206	34.95	23.7	0.42	74.9	97.0	41.44	0.15
I	1650	62.22	5.189	113.4	2.19	0.098	46.8	100.0	39.77	0.98
total gas age			$n = 9$		73.1	0.90			38.55	5.42*
plateau	MSWD = 1.4		$n = 3$	steps G–I	42.0	0.77		57.4	41.41	0.34*
isochron	MSWD = 109†		$n = 9$			$^{40}Ar/^{36}Ar = 278 \pm 33$*			**40.82**	**2.31***
9N20-1, G3:130, 21.37 mg whole rock, J = 0.000758201 ± 0.10%, NM-130, Lab# = 51781-01										
A √	*625*	*5094*	*0.1077*	*17022*	*1.68*	*4.7*	*1.3*	*0.6*	*86.0*	*96.9*
B √ ø	*700*	*240.4*	*0.2834*	*595.8*	*18.4*	*1.8*	*26.8*	*7.1*	*86.0*	*1.2*
C √ ø	*750*	*134.3*	*0.4443*	*168.4*	*12.1*	*1.1*	*63.0*	*11.4*	*112.19*	*0.56*
D √ ø	*800*	*117.2*	*1.012*	*117.7*	*9.59*	*0.50*	*70.4*	*14.8*	*109.51*	*0.51*
E √	*875*	*121.3*	*0.7859*	*150.0*	*8.64*	*0.65*	*63.5*	*17.9*	*102.43*	*0.61*
F	975	128.1	0.1523	167.0	29.2	3.4	61.5	28.3	104.64	0.44
G	1075	95.79	0.0806	65.64	65.8	6.3	79.8	51.7	101.60	0.25
H	1250	114.1	0.1642	127.9	106.4	3.1	66.9	89.5	101.54	0.39
I √	*1650*	*193.0*	*0.2512*	*380.6*	*29.6*	*2.0*	*41.7*	*100.0*	*106.95*	*0.75*
total gas age			$n = 9$		281.4	3.4			102.1	2.0*
plateau	MSWD = 20.1†		$n = 3$	steps F–H	201.4	4.2		71.6	**102.2**	**1.7***
isochron	MSWD = 7.5†		$n = 6$			$^{40}Ar/^{36}Ar = 308 \pm 9$*			100.5	1.7*

Table 3. (*continued*)

ID	T (°C)	$^{40}Ar/^{39}Ar$	$^{37}Ar/^{39}Ar$	$^{36}Ar/^{39}Ar$ $\times 10^{-3}$r	$^{39}Ar_K$ $\times 10^{-16}$ mol	K–Ca	$^{40}Ar^*$ (%)	^{39}Ar (%)	Age (Ma)	$\pm 1\sigma$ (Ma)
9N20-2, H9:130, 20.85 mg whole rock, J = 0.000751144 ± 0.10%, NM-130, Lab# = 51788-01										
A √	*625*	*295.6*	*0.0432*	*748.7*	*29.6*	*11.8*	*25.2*	*14.5*	*98.0*	*1.5*
B	700	93.24	0.0278	23.68	113.9	18.4	92.5	70.3	113.25	0.28
C	750	91.27	0.0473	15.94	42.6	10.8	94.8	91.2	113.66	0.24
D √	*800*	*85.61*	*0.1786*	*59.89*	*5.46*	*2.9*	*79.3*	*93.8*	*89.79*	*0.90*
E √	*875*	*100.0*	*0.1400*	*175.5*	*1.30*	*3.6*	*48.2*	*94.5*	*64.1*	*1.9*
F √	*975*	*193.2*	*0.2683*	*484.1*	*1.81*	*1.9*	*26.0*	*95.4*	*66.8*	*3.1*
G √	*1075*	*225.4*	*0.6308*	*653.7*	*1.17*	*0.81*	*14.3*	*95.9*	*43.2*	*4.8*
H √	*1250*	*319.5*	*0.6975*	*939.8*	*4.05*	*0.73*	*13.1*	*97.9*	*55.8*	*3.0*
I √	*1650*	*360.0*	*0.8578*	*1055*	*4.26*	*0.59*	*13.4*	*100.0*	*64.3*	*3.3*
total gas age			$n = 9$		204.2	14.4			107.2	1.3*
plateau	MSWD = 1.2		$n = 2$	steps B–C	156.6	16.3		76.7	113.5	0.6*
isochron	MSWD = 209†		$n = 9$			$^{40}Ar/^{36}Ar = 262 \pm 29$*			**113.5**	**5.8***
9N23-4, G6:130, 26.11 mg whole rock, J = 0.000757059 ± 0.10%, NM-130, Lab# = 51784-01										
A √	*625*	*28918*	*4.633*	*97322*	*0.223*	*0.11*	*0.6*	*0.2*	*207*	*3460*
B √	*700*	*1360*	*3.429*	*4044*	*2.12*	*0.15*	*12.1*	*1.9*	*212.9*	*15.5*
C √	*750*	*2480*	*6.351*	*7828*	*2.46*	*0.080*	*6.8*	*4.0*	*216.8*	*33.2*
D √	*800*	*1141*	*6.390*	*3230*	*3.09*	*0.080*	*16.4*	*6.5*	*240.5*	*10.8*
E √	*875*	*623.9*	*4.163*	*1423*	*4.75*	*0.12*	*32.6*	*10.4*	*259.5*	*4.1*
F ø	975	244.7	1.052	101.9	49.4	0.49	87.7	51.2	271.90	0.72
G ø	1075	246.8	1.517	91.10	21.5	0.34	89.1	69.0	278.23	0.59
H √ ø	*1250*	*295.6*	*4.203*	*199.1*	*15.1*	*0.12*	*80.2*	*81.4*	*298.90*	*0.99*
I √ ø	*1650*	*272.0*	*5.541*	*136.0*	*22.5*	*0.092*	*85.4*	*100.0*	*293.52*	*0.80*
total gas age			$n = 9$		121.1	0.30			276.8	16.8*
plateau	MSWD = 46.5†		$n = 2$	steps F–G	70.9	0.44		58.5	275.7	6.2*
isochron	MSWD = 0.8		$n = 5$			$^{40}Ar/^{36}Ar = 286 \pm 5$*			**274.2**	**13.4***
9N25-8, G2:130, 19.16 mg whole rock, J = 0.000760011 ± 0.10%, NM-130, Lab# = 51780-01										
A √	*625*	*3336*	*3.758*	*11051*	*0.886*	*0.14*	*2.1*	*0.9*	*94.4*	*113.6*
B √ ø	*700*	*434.7*	*1.371*	*1257*	*4.04*	*0.37*	*14.6*	*4.9*	*85.0*	*3.8*
C √	*750*	*404.1*	*3.651*	*1058*	*2.93*	*0.14*	*22.7*	*7.8*	*122.0*	*3.8*
D √	*800*	*357.8*	*4.427*	*898.9*	*3.46*	*0.12*	*25.9*	*11.3*	*123.0*	*3.1*
E √	*875*	*284.0*	*2.406*	*640.1*	*4.76*	*0.21*	*33.5*	*16.0*	*126.1*	*1.7*
F	975	125.3	0.9303	84.16	25.4	0.55	80.2	41.2	132.88	0.38
G	1075	122.4	0.6457	62.00	23.1	0.79	85.1	64.1	137.47	0.34
H	1250	143.6	1.938	145.9	21.3	0.26	70.1	85.3	133.19	0.55
I	1650	133.9	2.094	102.6	14.8	0.24	77.5	100.0	137.15	0.47
total gas age			$n = 9$		100.6	0.45			131.4	3.6*
plateau	MSWD = 36.8†		$n = 4$	steps F–I	84.6	0.49		84.0	135.4	2.5*
isochron	MSWD = 21.4†		$n = 8$			$^{40}Ar/^{36}Ar = 282 \pm 13$*			**136.9**	**2.6***
9N27-1, G4:130, 19.58 mg whole rock, J = 0.00075582 ± 0.10%, NM-130, Lab# = 51782-01										
A √	*625*	*1057*	*0.6491*	*3331*	*1.05*	*0.79*	*6.9*	*0.7*	*96.6*	*24.3*
B √ ø	*700*	*106.3*	*0.6236*	*166.2*	*9.92*	*0.82*	*53.8*	*7.7*	*76.44*	*0.56*
C	750	103.2	0.2780	59.62	8.97	1.8	83.0	14.1	113.12	0.42
D	800	96.64	0.3160	40.86	8.28	1.6	87.5	19.9	111.84	0.39
E	875	95.96	0.2382	42.25	8.05	2.1	87.0	25.6	110.43	0.39
F	975	95.41	0.4372	25.37	16.2	1.2	92.2	37.1	116.14	0.30
G	1075	86.23	0.6087	20.90	29.8	0.84	92.9	58.1	106.10	0.23
H	1250	95.42	2.546	40.57	51.5	0.20	87.7	94.4	110.83	0.24
I √ ø	*1650*	*151.5*	*1.715*	*85.57*	*7.88*	*0.30*	*83.4*	*100.0*	*164.79*	*0.58*
total gas age			$n = 9$		141.6	0.79			111.1	1.0*
plateau	MSWD = 153†		$n = 6$	steps C–H	122.8	0.83		86.7	110.6	3.1*
isochron	MSWD = 181†		$n = 7$			$^{40}Ar/^{36}Ar = 340 \pm 124$*			**108.8**	**7.0***

Table 3. (*continued*)

ID	T (°C)	$^{40}Ar/^{39}Ar$	$^{37}Ar/^{39}Ar$	$^{36}Ar/^{39}Ar$ $\times 10^{-3}$r	$^{39}Ar_K$ $\times 10^{-16}$ mol	K–Ca	$^{40}Ar^*$ (%)	^{39}Ar (%)	Age (Ma)	±1σ (Ma)
L9N16-2, G5:130, 18.34 mg whole rock, J = 0.000755249 ± 0.10%, NM-130, Lab# = 51783-01										
A √	*625*	*4403*	*3.433*	*14625*	*0.985*	*0.15*	*1.8*	*0.5*	*107.5*	*90.7*
B √	*700*	*213.1*	*1.635*	*376.4*	*9.29*	*0.31*	*47.9*	*5.5*	*134.1*	*1.0*
C √	*750*	*127.2*	*1.446*	*69.07*	*11.8*	*0.35*	*84.0*	*11.9*	*140.24*	*0.48*
D	800	122.2	1.124	48.77	17.9	0.45	88.3	21.5	141.47	0.36
E	875	125.9	0.6184	57.15	23.7	0.82	86.6	34.3	142.89	0.35
F	975	120.4	0.4278	38.81	44.7	1.2	90.5	58.3	142.73	0.28
G	1075	115.5	0.4663	23.72	38.1	1.1	94.0	78.8	142.24	0.26
H	1250	116.3	1.390	29.99	31.8	0.37	92.5	96.0	141.07	0.30
I	1650	121.8	3.185	50.00	7.50	0.16	88.1	100.0	140.92	0.50
total gas age			$n = 9$		185.8	0.77			141.4	1.7*
plateau	MSWD = 6.1†		$n = 6$	steps D–I	163.7	0.83		88.1	**142.0**	**0.7***
isochron	MSWD = 9.9†		$n = 9$			$^{40}Ar/^{36}Ar = 281 \pm 11$*			142.6	1.3*

Notes: Preferred ages are shown in **boldface**; *n*, number of heating steps; analyses in *italics* are excluded from final age calculations; √, analyses excluded from weighted mean age; ø, analyses excluded from inverse isochron age; K–Ca molar ratio calculated from reactor-produced ^{39}ArK and $^{37}ArCa$; isotopic ratios corrected for blank, radioactive decay and mass discrimination; not corrected for interfering reactions; individual analyses show analytical error only; plateau and total gas age errors include error in J and irradiation parameters; discrimination = 1.0069 ± 0.00099 a.m.u.

† MSWD outside of 95% confidence interval.

* 2σ error.

1994; Storey *et al.* 1999). The rifted margin is delimited sharply by the shelf-edge break where there is an abrupt increase in ocean depths to >1500 m (Fig. 1). It trends N58E. The N65E to N74E stretching direction is highly oblique to the rifted margin in western Marie Byrd Land and to crustal structures that were active there in middle Cretaceous time. One prevalent structural trend in the Ford Ranges is ESE, as exemplified by the Balchen Glacier Fault (Fig. 2; Siddoway *et al.* 2004*b*), and another is *c.* N30E (Fig. 2).

The regional pattern of dextral and sinistral faults (Fig. 2) and the regional stretching direction from dykes are compatible with transcurrent strain in the Ford Ranges in Early Cretaceous time (Fig. 8). As reported by Luyendyk *et al.* (2003), analysis of brittle faults in the Ford Ranges has revealed E–W-orientated dextral and NE-striking sinistral fault domains separating regions of predominantly normal faulting. Faults probably correspond with high amplitude, steep gradient aerogeophysical lineaments on Edward VII Peninsula (Ferraccioli *et al.* 2002) and parallel to the Ice Stream E (ISE) margin (Luyendyk *et al.* 2003). The ISE structure trends N30E toward the Ross/Amundsen Province boundary at Land Glacier, identified by Pankhurst *et al.* (1998) as the eastern limit of Palaeozoic, Ross-type crust in Marie Byrd Land. Potentially, the feature is a wrench fault that displaces the province boundary in Marie Byrd Land, as a rift-stage modification of the Mesozoic convergent margin.

The sole structural evidence for *c.* N–S stretching orthogonal to the western Marie Byrd Land margin comes from mafic dykes emplaced in the Fosdick Mountains dome (Fig. 5). The dyke orientations indicate *c.* NNE–SSW stretching (Richard *et al.* 1994), in conflict with the broad regional pattern determined from the variety of structural data presented in this paper. The dykes are late discordant features, judging from the sharp planar contacts and lack of foliation (Richard *et al.* 1994). They overprint kilometre-scale folds and penetrative ductile fabrics that do record NE extension; consequently, the Fosdick Mountains dykes are thought to have been emplaced during localized stretching and arching perpendicular to the dome axis as dome rocks were translated up into the brittle realm (Siddoway *et al.* 2004*b*). The single available dyke age of 96.4 ± 1.1 Ma (Table 2, sample Mutel-1; Richard *et al.* 1994) is consistent with the youngest dyke ages obtained in the broader Ford Ranges.

The broadly coeval $^{40}Ar/^{39}Ar$ results for Ford Ranges mafic dykes (this study), $^{40}Ar/^{39}Ar$ mineral ages for migmatite gneisses of the Fosdick Mountains (Richard *et al.* 1994) and $^{40}Ar/^{39}Ar$ and apatite fission track ages for shear zone rocks offshore in the Ross Sea (Fitzgerald & Baldwin 1997; Siddoway *et al.* 2004*a*) indicate

Table 4. Results of $^{40}Ar/^{39}Ar$ analysis of biotite and muscovite mineral separates

ID	T (°C)	$^{40}Ar/^{39}Ar$	$^{37}Ar/^{39}Ar$	$^{36}Ar/^{39}Ar$ $\times 10^{-3}$r	$^{39}Ar_K$ $\times 10^{-16}$ mol	K–Ca	$^{40}Ar^*$ (%)	^{39}Ar (%)	Age (Ma)	±1σ (Ma)
9D7-4, #21:131, 2.74 mg biotite, J = 0.003906654 ± 0.10%, NM-131, Lab# = 51800-01										
A √ ø	*650*	*34.61*	*0.0447*	*85.82*	*3.05*	*11.4*	*26.7*	*0.6*	*63.9*	*2.6*
B √	*750*	*16.66*	*0.0245*	*8.020*	*29.1*	*20.8*	*85.6*	*5.9*	*97.86*	*0.34*
C	850	14.36	0.0115	1.109	112.8	44.5	97.6	26.7	96.11	0.18
D	920	14.36	0.0202	0.5398	74.1	25.2	98.7	40.4	97.28	0.19
E	1000	14.49	0.0273	1.042	43.8	18.7	97.7	48.5	97.17	0.19
F	1075	14.42	0.0089	0.9642	125.3	57.4	97.9	71.6	96.81	0.20
G	1110	14.30	0.0127	0.4755	67.3	40.3	98.9	84.0	97.01	0.17
H	1180	14.48	0.0438	1.130	38.8	11.7	97.6	91.2	96.93	0.20
I	1210	14.36	0.0793	0.6810	15.1	6.4	98.5	94.0	97.03	0.31
J	1250	14.30	0.3072	0.8008	21.6	1.7	98.4	98.0	96.54	0.27
K	1300	14.56	0.6420	1.437	10.2	0.79	97.3	99.8	97.20	0.41
L √ ø	*1675*	*33.90*	*2.618*	*70.27*	*0.879*	*0.19*	*39.3*	*100.0*	*91.7*	*5.9*
total gas age			*n* = 12		542.2	7.8			96.66	0.46*
plateau	MSWD = 3.4†		*n* = 9	steps C–K	509.2	21.6		93.9	**96.92**	**0.34***
isochron	MSWD = 4.5†		*n* = 10			$^{40}Ar/^{36}Ar$ = 313 ± 29*			96.79	0.52†
L9N15-1, #23:131, 2.26 mg muscovite, J = 0.003896088 ± 0.10%, NM-131, Lab# = 51798-01										
A √ ø	*600*	*98.12*	*0.1650*	*204.2*	*0.943*	*3.1*	*38.5*	*0.2*	*247.7*	*8.3*
B √ ø	*650*	*51.76*	*0.4693*	*19.31*	*1.01*	*1.1*	*89.0*	*0.3*	*298.0*	*3.7*
C √ ø	*700*	*52.64*	*0.3218*	*5.838*	*1.77*	*1.6*	*96.7*	*0.7*	*326.5*	*2.2*
D √	*775*	*56.00*	*0.0319*	*8.969*	*4.19*	*16.0*	*95.2*	*1.4*	*340.6*	*1.2*
E √	*825*	*56.84*	*0.0124*	*8.310*	*9.89*	*41.0*	*95.6*	*3.2*	*346.59*	*0.95*
F	875	54.93	0.0015	4.522	20.1	330.0	97.5	6.8	341.95	0.71
G	900	54.27	0.0008	1.847	28.2	662.8	98.9	11.8	342.72	0.60
H	950	53.81	0.0017	0.8559	122.8	293.4	99.5	33.7	341.74	0.62
I	1010	53.58	0.0014	0.7323	99.1	362.0	99.5	51.4	340.63	0.73
J	1050	54.06	0.0000	0.7795	58.9	—	99.5	61.9	343.31	0.54
K	1100	53.79	0.0010	0.2644	141.3	492.4	99.8	87.1	342.67	0.64
L	1150	53.92	0.0025	0.3801	60.2	202.2	99.7	97.8	343.22	0.63
M √	*1225*	*55.45*	*0.0133*	*4.105*	*5.30*	*38.5*	*97.8*	*98.8*	*345.7*	*1.2*
N √	*1350*	*54.69*	*0.0686*	*4.798*	*2.42*	*7.4*	*97.4*	*99.2*	*340.1*	*1.9*
O √	*1680*	*58.48*	*0.3175*	*15.98*	*4.36*	*1.6*	*91.9*	*100.0*	*343.1*	*1.5*
total gas age			*n* = 15		560.6	17.1			342.0	1.4*
plateau	MSWD = 2.1		*n* = 7	steps F–L	530.7	368.7		94.7	**342.4**	**1.0***
isochron	MSWD = 4.3†		*n* = 12			$^{40}Ar/^{36}Ar$ = 320 ± 48*			342.4	1.6†
L9N17-2, #22:131, 1.59 mg muscovite, J = 0.003905434 ± 0.10%, NM-131, Lab# = 51799-01										
A √	*600*	*122.7*	*0.0287*	*296.4*	*0.503*	*17.8*	*28.6*	*0.1*	*231.5*	*16.1*
B √	*650*	*57.96*	*0.2635*	*65.42*	*0.948*	*1.9*	*66.6*	*0.4*	*253.5*	*5.2*
C √	*700*	*50.47*	*1.046*	*13.32*	*1.61*	*0.49*	*92.3*	*0.8*	*301.9*	*2.6*
D √	*775*	*55.26*	*0.2712*	*12.96*	*3.50*	*1.9*	*93.1*	*1.6*	*330.3*	*1.5*
E √	*825*	*56.06*	*0.0322*	*7.290*	*7.31*	*15.8*	*96.1*	*3.4*	*344.6*	*1.0*
F	875	55.51	0.0202	3.684	15.7	25.2	98.0	7.3	347.56	0.79
G	900	55.11	0.0137	1.724	27.4	37.1	99.0	14.1	348.56	0.65
H	950	54.62	0.0088	0.6608	80.4	58.2	99.6	34.0	347.57	0.51
I	1010	54.63	0.0170	0.7568	49.1	29.9	99.5	46.1	347.44	0.60
J	1050	54.92	0.0141	0.9275	23.6	36.1	99.5	52.0	348.84	0.73
K	1100	54.89	0.0113	0.8607	61.0	45.1	99.5	67.0	348.78	0.62
L	1150	54.80	0.0060	0.8668	90.4	85.2	99.5	89.4	348.25	0.73
M	1225	55.81	0.0779	4.337	26.7	6.5	97.7	96.0	348.18	0.67
N √	*1350*	*54.10*	*0.4885*	*11.82*	*5.84*	*1.0*	*93.6*	*97.5*	*325.6*	*1.5*
O √	*1720*	*56.15*	*0.2291*	*13.75*	*10.2*	*2.2*	*92.8*	*100.0*	*334.1*	*1.1*
total gas age			*n* = 15		404.1	13.8			346.7	1.4*
plateau	MSWD = 0.8		*n* = 8	steps F–M	374.2	28.4		92.6	**348.2**	**0.9***
isochron	MSWD = 62.5†		*n* = 15			$^{40}Ar/^{36}Ar$ = 185 ± 63*			348.0	5.7*

Table 4. (*continued*)

ID	T (°C)	$^{40}Ar/^{39}Ar$	$^{37}Ar/^{39}Ar$	$^{36}Ar/^{39}Ar$ $\times 10^{-3}$r	$^{39}Ar_K$ $\times 10^{-16}$ mol	K–Ca	$^{40}Ar^*$ (%)	^{39}Ar (%)	Age (Ma)	±1σ (Ma)
L9N17-3, #26:131, 1.07 mg muscovite, J = 0.003885327 ± 0.10%, NM-131, Lab# = 51795-01										
A √ ø	*600*	*99.46*	*2.863*	*236.4*	*0.563*	*0.18*	*30.0*	*0.2*	*198.2*	*11.2*
B √ ø	*650*	*68.72*	*1.914*	*102.5*	*0.627*	*0.27*	*56.1*	*0.5*	*252.2*	*7.0*
C √ ø	*700*	*60.19*	*3.315*	*33.33*	*0.872*	*0.15*	*84.1*	*0.9*	*324.5*	*4.7*
D √	*775*	*60.98*	*0.8047*	*20.76*	*2.15*	*0.63*	*90.0*	*1.8*	*348.9*	*2.1*
E	825	57.31	0.0569	8.093	5.13	9.0	95.8	4.0	348.8	1.2
F	875	56.63	0.0264	6.500	10.2	19.3	96.6	8.3	347.58	0.83
G	925	55.37	0.0111	2.371	39.4	46.1	98.7	25.1	347.32	0.63
H	975	55.27	0.0075	1.547	35.0	67.7	99.1	40.0	348.19	0.58
I	1010	55.34	0.0344	1.837	11.1	14.8	99.0	44.7	348.07	0.74
J	1050	55.05	0.0141	1.821	21.1	36.2	99.0	53.7	346.42	0.59
K	1150	54.99	0.0044	1.866	88.7	116.6	99.0	91.5	346.01	0.58
L ø	1250	58.17	0.0750	13.85	8.29	6.8	92.9	95.0	344.0	1.0
M √ ø	*1400*	*58.58*	*0.7182*	*19.51*	*3.61*	*0.71*	*90.2*	*96.6*	*337.1*	*1.6*
N √	*1650*	*60.66*	*0.4963*	*21.79*	*8.02*	*1.0*	*89.4*	*100.0*	*345.1*	*1.1*
total gas age			$n = 14$		234.7	2.0			345.9	1.5*
plateau	MSWD = 3.2†		$n = 8$	steps E–L	218.9	21.6		93.3	**347.3**	**1.2***
isochron	MSWD = 2.7†		$n = 9$			$^{40}Ar/^{36}Ar = 289 \pm 26$*			347.3	1.4*
L9N17-3, #25:131, 3.18 mg biotite, J = 0.003886951 ± 0.10%, NM-131, Lab# = 51796-01										
A √ ø	*650*	*26.20*	*0.1509*	*21.53*	*15.1*	*3.4*	*75.7*	*2.2*	*133.92*	*0.69*
B	750	56.70	0.1181	5.410	56.5	4.3	97.2	10.6	350.08	0.59
C	850	55.10	0.0082	0.4764	172.7	62.1	99.7	36.2	349.19	0.67
D	920	55.60	0.0071	0.3149	63.2	71.8	99.8	45.5	352.35	0.53
E √	*1000*	*57.50*	*0.0256*	*0.7312*	*61.3*	*19.9*	*99.6*	*54.6*	*362.55*	*0.62*
F √	*1075*	*56.46*	*0.0145*	*0.4203*	*144.1*	*35.1*	*99.7*	*75.9*	*357.13*	*0.76*
G √	*1110*	*55.81*	*0.0153*	*0.4660*	*69.5*	*33.4*	*99.7*	*86.2*	*353.30*	*0.55*
H √	*1180*	*55.69*	*0.0673*	*0.7395*	*42.5*	*7.6*	*99.6*	*92.5*	*352.18*	*0.59*
I √	*1210*	*56.14*	*0.1015*	*2.109*	*17.4*	*5.0*	*98.9*	*95.1*	*352.48*	*0.87*
J √	*1250*	*55.39*	*0.4494*	*0.6459*	*14.2*	*1.1*	*99.7*	*97.2*	*350.87*	*0.69*
K √	*1300*	*56.11*	*0.4601*	*1.170*	*10.0*	*1.1*	*99.4*	*98.7*	*354.17*	*0.81*
L √	*1675*	*57.48*	*0.5389*	*8.406*	*8.99*	*0.95*	*95.7*	*100.0*	*349.77*	*0.87*
total gas age			$n = 12$		675.7	5.2			348.5	1.3*
plateau	MSWD = 8.0†		$n = 3$	steps B–D	292.5	12.2		43.3	**350.8**	**2.1***
isochron	MSWD = 43.4†		$n = 11$			$^{40}Ar/^{36}Ar = 191 \pm 104$*			354.2	4.9*

Notes: Preferred ages are shown in **boldface**; *n*, number of heating steps; analyses in *italics* are excluded from final age calculations; √, analyses excluded from weighted mean age; ø, analyses excluded from inverse isochron age; K–Ca molar ratio calculated from reactor produced $^{39}Ar_K$ and $^{37}ArCa$; isotopic ratios corrected for blank, radioactive decay and mass discrimination; not corrected for interfering reactions; individual analyses show analytical error only; plateau and total gas age errors include error in J and irradiation parameters; discrimination = 1.0069 ± 0.00099 a.m.u.

† MSWD outside of 95% confidence interval.

* 2σ error.

dynamic events in western Marie Byrd Land at *c.* 100 Ma to 95 Ma, and the kinematic data now available for the Ford Ranges suggest that they involved transcurrent motions, presumably linked to activity along the Gondwana margin (Fig. 10). The kinematics and timing are consistent with structural and age evidence for dextral shearing at *c.* 103 Ma in Ellsworth Land to the east (Vaughan & Storey 2000; Vaughan *et al.* 2002). Thus, the onshore record in West Antarctica, based on the western Marie Byrd Land and Ellsworth Land sites, lends support to the model for dextral oblique convergence along the Cretaceous Gondwana margin, proposed by Sutherland & Hollis (2001).

The $^{40}Ar/^{39}Ar$ results for Ford Ranges mafic dykes are broadly coeval with $^{40}Ar/^{39}Ar$ mineral ages for migmatite gneisses of the Fosdick Mountains determined by Richard *et al.* (1994). Some samples from Marie Byrd Land sites (Edward VII Peninsula, Lisker & Olesch 1998; and Fosdick Mountains, Richard *et al.* 1994) yield apatite fission track data that also reflect an event at *c.* 100 Ma; however, in the region

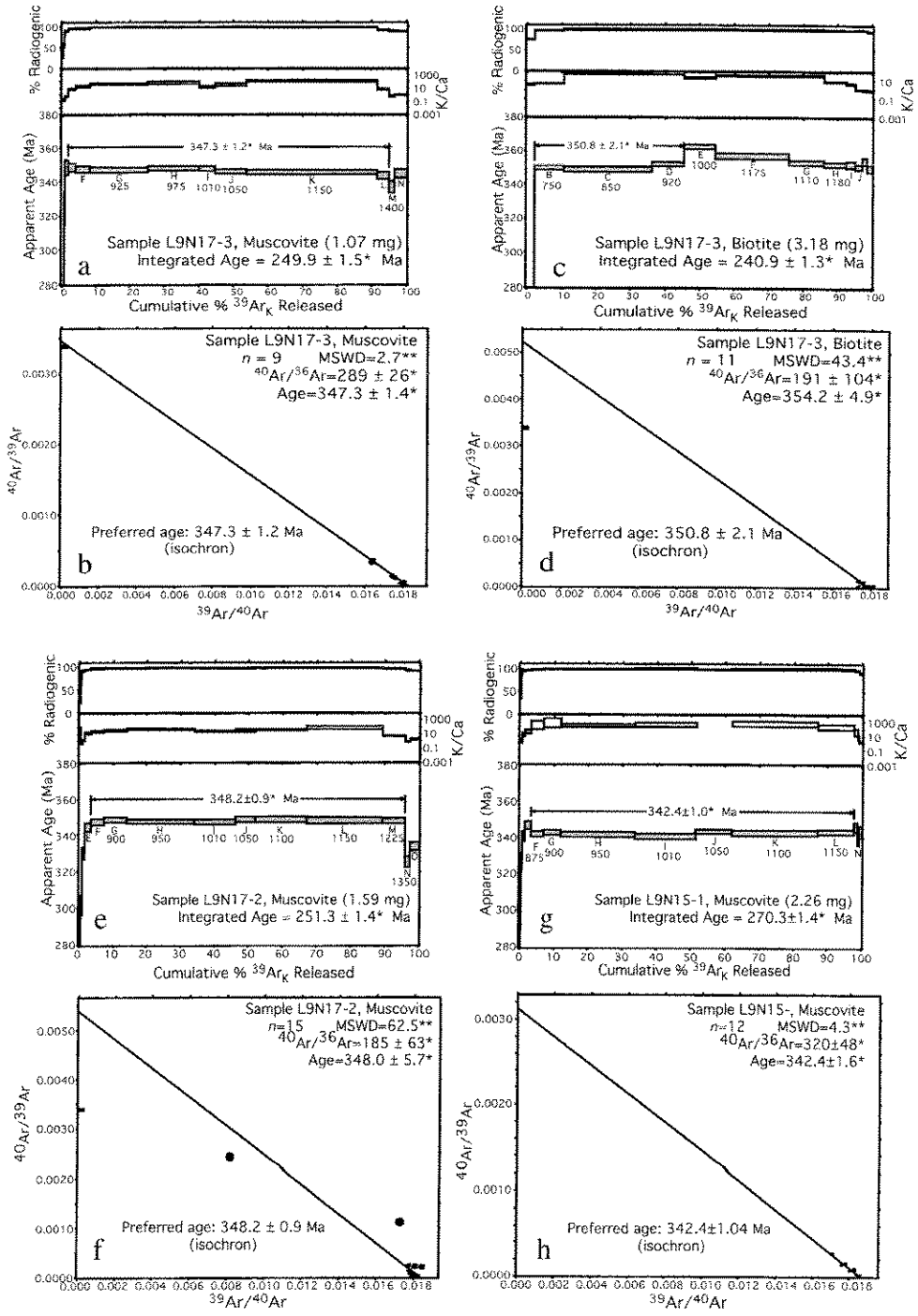

Fig. 7. $^{40}Ar/^{39}Ar$ age spectra and inverse isochron diagrams for muscovite and biotite mineral separates from samples of wall rock of the Ford Granodiorite suite. (**a**, **b**) Sample L9N17-3, muscovite; (**c**, **d**) sample L9N17-3, biotite; (**e**, **f**) sample L9N17-2, muscovite; (**g**, **h**) sample L9N15-1, muscovite. Preferred age is noted within the inverse isochron frames. All errors are reported at 2σ.

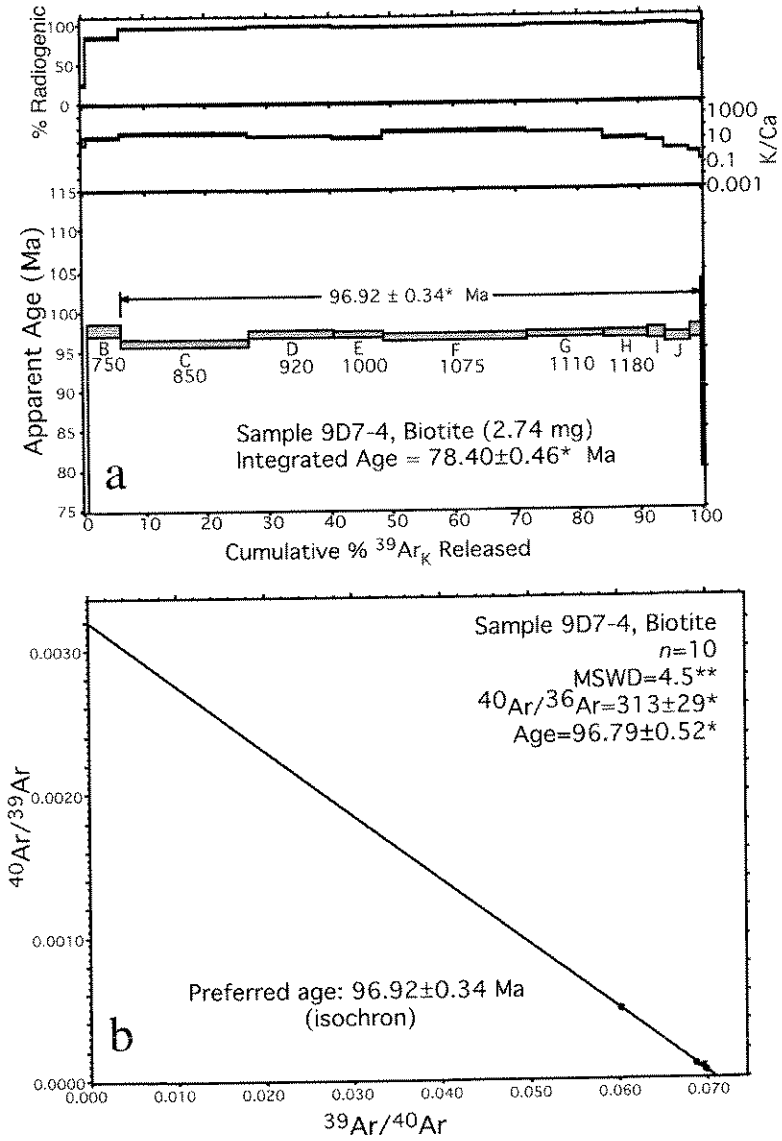

Fig. 8. $^{40}Ar/^{39}Ar$ results for biotite sample 9D7-4 comes from a mylonitic shear zone cutting Ford Granodiorite. The biotite is recrystallized dynamically within the shear zone and is considered to be syn-tectonic in the zone. (**a**) Age spectra; (**b**) inverse isochron diagram. Errors are reported at 2σ.

there is fairly clear apatite fission track evidence for rapid transit through the partial annealing zone at *c.* 80–70 Ma (Richard *et al.* 1994; Lisker & Olesch 1998; Siddoway *et al.* 2004*a*). Thus, there are indications of a tectonically quiet interval followed by a denudation and rapid cooling event at 71–75 Ma (Richard *et al.* 1994; Lisker & Olesch 1998; Siddoway *et al.* 2004*a*). The younger apatite fission track ages seem to be the sole indication, in Marie Byrd Land, of differential fault movements at the time of rifting between Marie Byrd Land and the Campbell Plateau of New Zealand during Late Cretaceous time. Seafloor spreading commenced around 79 Ma (Stock & Cande 2002). The fairly rapid onset of seafloor spreading and the abrupt rifted margin defined by the –1500 m bathymetric contour in Marie Byrd

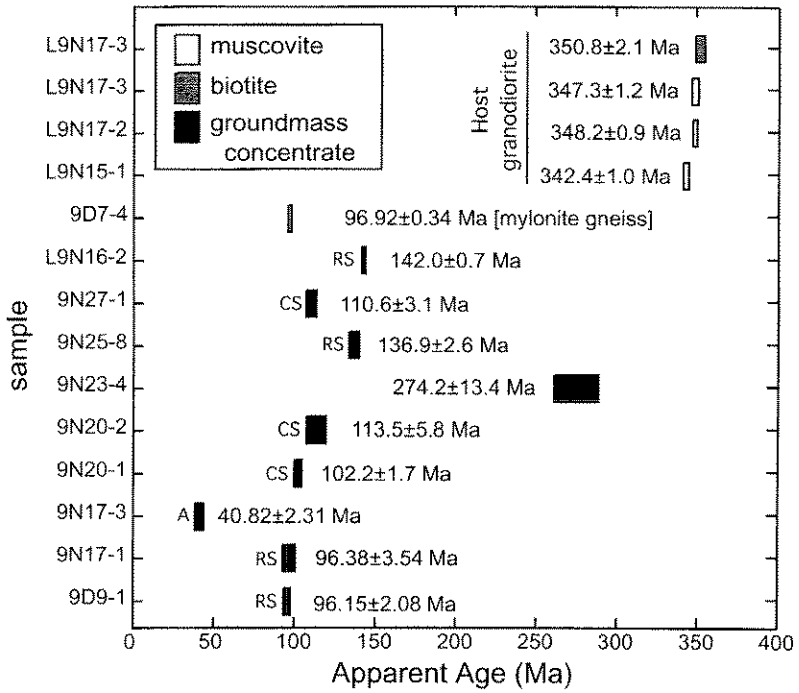

Fig. 9. Summary diagram of all $^{40}Ar/^{39}Ar$ ages. From top to bottom, the figure shows first a group of mica ages of >342 Ma; these correspond to host rocks of the Ford Granodiorite suite. The remaining $^{40}Ar/^{39}Ar$ biotite age in line 5 is the result from biotite involved in mylonitic shear zones at Mt Cooper. The nine groundmass concentrate ages are for dolerite dykes. Those labelled 'RS' yielded initial anomalously young apparent ages at the lowest temperature steps during analysis, followed by monotonically increasing ages at the intermediate to highest temperature steps. Those labelled 'CS' have complex saddle-, hump-, or stair-shaped spectra. For both 'RS' and 'CS' spectra, high K–Ca ratios generally coincide with older apparent ages.

Land and Campbell Plateau (Fig. 1) are possible signs that seafloor spreading commenced upon a pre-existing structure such as a transcurrent fault.

The early phase of ENE stretching, recorded by the new kinematic data from western Marie Byrd, is attributed to a transcurrent strain field associated with dextral strike-slip along the Cretaceous Gondwana margin. It is hypothesized that the sharp rifted margin and the principal structural grain on land were established through strike-slip parallel to the Gondwana margin. The stretching direction determined from dyke geometries is kinematically consistent with the interpreted movements upon dextral *c.* E–W faults and sinistral NW–SE faults, active at the same time, at *c.* 100 Ma. The orthogonal rifting between the Campbell Plateau of New Zealand and Marie Byrd Land did occur *c.* 20 Ma later. Thus, modification of the Gondwana margin was accomplished in two stages (cf. Richard *et al.* 1994).

Conclusions

Mafic dykes in the Ford Ranges have $^{40}Ar/^{39}Ar$ ages of 142 Ma to 96 Ma and record crustal stretching orientated ENE–WSW (azimuth *c.* 070–250), orthogonal to dyke margins. Although some age determinations have large errors due to argon loss caused by alternation of groundmass, the $^{40}Ar/^{39}Ar$ results nonetheless establish the middle Cretaceous timing of mafic dyke emplacement with some certainty. Diverse types of structural data support the kinematic interpretation of transcurrent strain along and inboard of the Gondwana margin.

The recognition of transcurrent structures in Marie Byrd Land preceding break-up of the margin may explain key features of the Marie Byrd Land rifted margin, namely: (1) the rifted margin cuts at a high angle across Ross Sea basins (Lawver & Gahagan 1994); (2) the rifted margin is exceptionally linear (Sutherland 1999); and (3) no evidence is found in the Ford

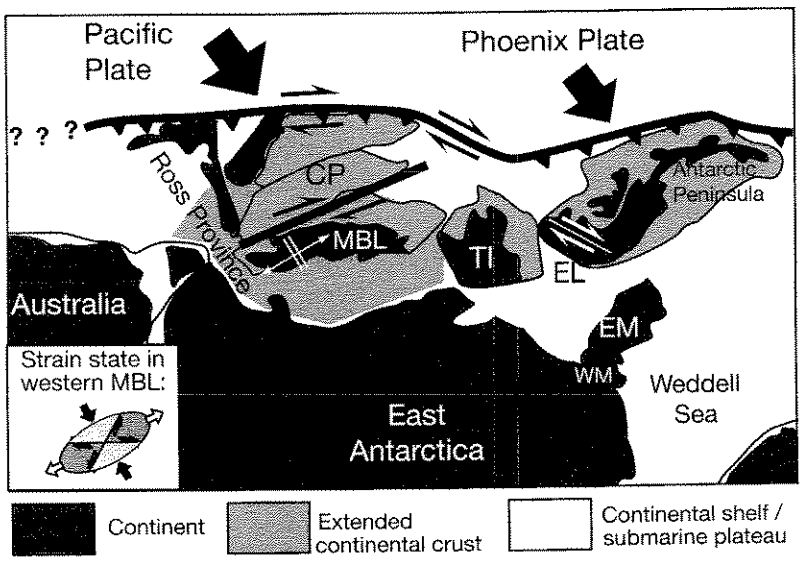

Fig. 10. Tectonic model of a transcurrent setting for the Gondwana margin and western Marie Byrd Land, associated with oblique convergence. The ENE to NE stretching direction interpreted from mafic dykes and other Ford Ranges structures is consistent with dextral transcurrent deformation along the margin. Abbreviations are as follows: CP, Campbell Plateau; MBL, Marie Byrd Land; TI, Thurston Island; EM, Ellsworth Mountains; WM, Whitmore Mountains. Dextral shear indication in Antarctic Peninsula is after Vaughan *et al.* (1999).

Ranges for distributed deformation or magmatism at the time of break-up (Siddoway *et al.* 2004*a*). The absence of contractional structures and 'rift' sediments is also consistent with a transcurrent strain environment and an oblique orientation of the minimum finite strain axis with respect to major structures. To test this hypothesis, future work will involve integration of geological results with the airborne geophysics dataset for the region and comparison of kinematic data from the Ford Ranges to more distant sites in Marie Byrd Land (e.g. Storey *et al.* 1999), on the Antarctic Peninsula (e.g. Vaughan & Storey 2000; Vaughan *et al.* 1999), and on the western Ross Sea margin (e.g. Wilson 1995; Salvini *et al.* 1997). The 'longitudinal convergence problem' means that such a task will not be straightforward. Direct comparison to structural/geophysical data from other Antarctic regions can be accomplished best when the data are converted to the coordinates of the Antarctic navigational grid (Airforce & Navy 1973) according to the modular conversion: AGN strike = MOD [(latitude position at study site + strike of structure with respect to true north), 360]. The formula is generally applicable, irrespective of longitude. An advantage of this normalization is that Antarctic navigational grid data can be compared directly with aeromagnetic and other geophysical trends plotted in polar stereographic grid coordinates. The geochemistry of the western Marie Byrd Land dyke array should also be investigated, in order to address the hypothesis that a mantle plume was active in the region and influenced the rifting process in Marie Byrd Land (Weaver *et al.* 1994; Storey *et al.* 1999).

Funding is from United States National Science Foundation grant OPP-9615282 to C. Siddoway. S. Richard, A. Whitehead, S. Cowdery, M. Roberts & R. Meyer contributed to collection of field data. V. DiVenere, B. Storey, A. Vaughan & I. Dalziel provided helpful reviews. Stereographs were prepared using Stereonet v. 6.2.X [1988–2002] by R. W. Allmendinger, and Faultkin v. 4.1.0 software [2002] by R.W. Allmendinger, R. A. Marrett & T. Cladouhos.

References

ADAMS, C.J., SEWARD, D. & WEAVER, S.D. 1995. Geochronology of Cretaceous granites and metasedimentary basement on Edward VII Peninsula, Marie Byrd Land, West Antarctica. *Antarctic Science*, **7**, 265–277.

AIR FORCE, DEPARTMENT OF, AND NAVY, DEPARTMENT OF, 1973. *Grid Navigation, Air Navigation,*

Volume AFM 51-40; NAVAIR 00-80V-49: Flight Training. Air Training Command, United States Government Printing Office, Washington, D.C., Chapter 19, 1–14.

BEST, M.G. 1988. Early Miocene changes in direction of least principal stress, southwestern United States: conflicting inferences from dikes and metamorphic core-detachment fault terranes. *Tectonics*, **7**, 249–259.

BRADSHAW, J.D., ANDREW, P.B. & FIELD, B.D. 1983. Swanson Formation and related rocks of Marie Byrd Land and a comparison with the Robertson Bay Group of northern Victoria Land. *In*: OLIVER, R.L., JAMES, P.R. & JAGO, J.B. (eds) *Antarctic Earth Science*. Cambridge University Press, Cambridge, 274–279.

BRADSHAW, J.D., PANKHURST, R.J., WEAVER, S.D., STOREY, B.C., MUIR, R.J. & IRELAND, T.R. 1997. New Zealand superterranes recognized in Marie Byrd Land and Thurston Island. *In*: RICCI, C.A. (ed.) *The Antarctic Region: Processes and Evolution*. Terra Antartica Publications, Siena, 429–436.

DALZIEL, I.W.D. & ELLIOT, D.H. 1982. West Antarctica: problem child of Gondwanaland. *Tectonics*, **1**, 3–19.

DEINO, A. & POTTS, R. 1990. Single-Crystal $^{40}Ar/^{39}Ar$ dating of the Olorgesailie Formation, Southern Kenya Rift. *Journal of Geophysical Research*, **95**, 8453–8470.

DIVENERE, V., KENT, D.V. & DALZIEL, I.W.D. 1994. Mid-Cretaceous paleomagnetic results from Marie Byrd Land, West Antarctica: A test of post-100 Ma relative motion between East and West Antarctica. *Journal of Geophysical Research*, **99**, 15 115–15 139.

FERRACCIOLI, F., BOZZO, E. & DAMASKE, D. 2002. Aeromagnetic signatures over western Marie Byrd Land provide insight into magmatic arc basement, mafic magmatism and structure of the eastern Ross Sea Rift flank. *Tectonophysics*, **347**, 139–165.

FITZGERALD, P.G. & BALDWIN, S. 1997. Detachment fault model for evolution of the Ross Embayment. *In*: RICCI, C.A. (ed.) *The Antarctic Region: Processes and Evolution*. Terra Antartica Publications, Siena, 555–564.

FOLAND, K.A., FLEMING, T.H., HEIMANN, A. & ELLIOT, D.H. 1993. Potassium–Argon dating of fine-grained basalts with massive Ar loss: application of the $^{40}Ar/^{39}Ar$ technique to plagioclase and glass from the Kirkpatrick Basalt, Antarctica. *Chemical Geology*, **107**, 173–190.

IRELAND, T.R., BRADSHAW, J.D., MUIR, R.J., WEAVER, S.D. & ADAMS, C.J. 1994. Zircon age distributions in granites, greywackes, and gneisses from the southwest Pacific Gondwana Region. *U.S. Geological Survey Circular*, **1107**, 151.

LAWVER, L.A. & GAHAGAN, L.M. 1994. Constraints on timing of extension in the Ross Sea Region. *Terra Antartica*, **1**, 545–552.

LISKER, F. & OLESCH, M. 1998. Cooling and denudation history of western Marie Byrd Land, Antarctica, based on apatite fission-tracks. *In*: VAN DEN HAUTE, P. & DE CORTE, F. (eds) *Advances in Fission-Track Geochronology*. Kluwer Academic Publishers, The Netherlands, 225–240.

LUYENDYK, B.P., RICHARD, S.M., SMITH, C.H. & KIMBROUGH, D.L. 1992. Geological and geophysical investigations in the northern Ford Ranges, Marie Byrd Land, West Antarctica. *In*: YOSHIDA, Y., KAMINUMA, K. & SHIRAISHI, K. (eds) *Recent Progress in Antarctic Earth Science*. Terra Publications, Tokyo, Japan, 279–288.

LUYENDYK, B.P., CISOWSKI, S., SMITH, C.H., RICHARD, S.M. & KIMBROUGH, D.L. 1996. Paleomagnetic study of the northern Ford Ranges, western Marie Byrd Land, West Antarctica: a middle Cretaceous pole, and motion between West and East Antarctica? *Tectonics*, **15**, 122–141.

LUYENDYK, B.P., SORLIEN, C.C., WILSON, D., BARTEK, L., ELY, G., SIDDOWAY, C.S. & ZELLMER, K. 2001. Structural and tectonic evolution of the Ross Sea rift in the Cape Colbeck region, Eastern Ross Sea, Antarctica. *Tectonics*, **20**, 6, 933–958.

LUYENDYK, B.P., WILSON, D. & SIDDOWAY, C.S. 2003. The eastern margin of the Ross Sea Rift in western Marie Byrd Land: Crustal structure and tectonic development. *Geochemistry, Geophysics, Geosystems (G^3)*, **4** (10), 1090, doi:10.1029/2002GC000462.

MAHON, K.I. 1996. The New 'York' regression: Application of an improved statistical method to geochemistry. *International Geology Review*, **38**, 293–303.

MUIR, R.J., IRELAND, T.R., WEAVER, S.D. & BRADSHAW, J.D. 1994. Ion microprobe U–Pb zircon geochronology of granitic magmatism in the Western Province of the South Island, New Zealand. *Chemical Geology*, **113**, 171–189.

PANKHURST, R.J., WEAVER, S.D., BRADSHAW, J.D., STOREY, B.C. & IRELAND, T.R. 1998. Geochronology and geochemistry of pre-Jurassic superterranes in Marie Byrd Land, Antarctica. *Journal of Geophysical Research*, **B2**, **103**, 2529–2547.

RICHARD, S.M., SMITH, C.H., KIMBROUGH, D.L., FITZGERALD, P.G. & LUYENDYK, B.P. 1994. Cooling history of the northern Ford Ranges, Marie Byrd Land, West Antarctica. *Tectonics*, **13**, 837–857.

SALVINI, F., BRANCOLINI, G., BUSETTI, M., STORTI, F., MAZZARINI, F. & COREN, F. 1997. Cenozoic geodynamics of the Ross Sea Region, Antarctica: Crustal extension, intraplate strike-slip faulting and tectonic inheritance. *Journal of Geophysical Research*, **102**, 24 669–24 696.

SAMSON, S.D. & ALEXANDER, E.C., JR. 1987. Calibration of the interlaboratory $^{40}Ar/^{39}Ar$ dating standard, Mmhb-1. *Chemical Geology*, **66**, 27–34.

SIDDOWAY, C., BALDWIN, S., FITZGERALD, P.G., FANNING, C.M., & LUYENDYK, B.P. 2004*a*. Ross Sea mylonites and the timing of intracontinental extension within the West Antarctic rift system. *Geology*, **32**, 1, 57–60.

SIDDOWAY, C., RICHARD, S., FANNING, C.M. & LUYENDYK, B.P. 2004*b*. Origin and emplacement mechanisms for a middle Cretaceous gneiss dome, Fosdick Mountains, West Antarctica. *In*: WHITNEY, D., TEYSSIER, C.T. & SIDDOWAY, C.

(eds) *Gneiss domes and orogeny*. Geological Society of America Special Paper **380**, 267–294.

STEIGER, R.H. & JÄGER, E. 1977. Subcommission on geochronology: Convention on the use of decay constants in geo- and cosmochronology. *Earth and Planetary Science Letters*, **36**, 359–362.

STOCK, J.M. & CANDE, S. C. 2002. Tectonic history of Antarctic seafloor in the Australia–New Zealand–South Pacific sector: Implications for Antarctic continental tectonics. *In*: GAMBLE, J., SKINNER, D., HENRYS, S. & LYNCH, R. (eds) *Proceedings of 8th International Symposium on Antarctic Earth Sciences*. Royal Society of New Zealand Bulletin, **35**, Wellington, New Zealand, 251–259.

STOREY, B.C., DALZIEL, I.W.D., GARRETT, S.W., GRUNOW, A.M., PANKHURST, R.J. & VENNUM, W.R. 1988. West Antarctica in Gondwanaland: crustal blocks, reconstruction and break-up processes. *Tectonophysics*, **155**, 381–390.

STOREY, B.C., LEAT, P.T., WEAVER, S.D., PANKHURST, J.D. & KELLEY, S. 1999. Mantle plumes and Antarctica–New Zealand rifting: evidence from mid-Cretaceous mafic dykes. *Journal of the Geological Society, London*, **156**, 659–671.

SUTHERLAND, R. 1999. Basement geology and tectonic development of the greater New Zealand region: An interpretation from regional magnetic data. *Tectonophysics*, **308**, 341–362.

SUTHERLAND, R. & HOLLIS, C. 2001, Cretaceous demise of the Moa plate and strike-slip motion at the Gondwana margin. *Geology*, **29**, 279–282.

TAYLOR, J.R. 1982. *An Introduction to Error Analysis: The Study of Uncertainties in Physical Measurements*. University Science Books, Mill Valley, California, 270.

TSUNAKAWA, H. 1983. Simple two-dimensional model of propagation of magma-filled cracks. *Journal of Volcanology and Geothermal Research*, **16**, 335–342.

VAUGHAN, A.P.M. & STOREY, B.C. 2000. The eastern Palmer Land shear zone: a new terrane accretion model for the Mesozoic development of the Antarctic Peninsula. *Journal of the Geological Society, London*, **157**, 1243–1256.

VAUGHAN, A.P.M., MILLAR, I.L. & THISTLEWOOD, L. 1999. The Auriga Nunataks shear zone: Mesozoic transfer faulting and arc deformation in northwest Palmer Land, Antarctica. *Tectonics*, **18**, 911–928.

VAUGHAN, A.P.M., PANKHURST, R.J. & FANNING, C.M. 2002. A mid-Cretaceous age for the Palmer Land event, Antarctic Peninsula: implications for terrane accretion timing and Gondwana palaeolatitudes. *Journal of the Geological Society, London*, **159**, 113–116.

WEAVER, S.D., BRADSHAW, J.D. & ADAMS, C.J. 1991. Granitoids of the Ford Ranges, Marie Byrd Land, Antarctica. *In*: THOMSON, M.R.A., CRAME, J.A. & THOMSON, J.W. (eds) *Geological Evolution of Antarctica*. Cambridge University Press, Cambridge, 345–351.

WEAVER, S.D., ADAMS, C.J., PANKHURST, R.J. & GIBSON, I.L. 1992. Granites of Edward VII Peninsula, Marie Byrd Land: anorogenic magmatism related to Antarctic–New Zealand rifting. *Transactions of the Royal Society of Edinburgh*, **83**, 281–290.

WEAVER, S.D., STOREY, B.C., PANKHURST, R.J., MUKASA, S.B., DIVENERE, V.J. & BRADSHAW, J.D. 1994. Antarctica–New Zealand rifting and Marie Byrd Land lithospheric magmatism linked to ridge subduction and mantle plume activity. *Geology*, **22**, 811–814.

WILSON, T. 1995. Cenozoic transtension along the Transantarctic Mountains–West Antarctic rift boundary, southern Victoria Land, Antarctica. *Tectonics*, **14**, 531–545.

YORK, D. 1969. Least squares fitting of a straight line with correlated errors. *Earth and Planetary Science Letters*, **5**, 320–324.